



CERN-EP-2020-027
 LHCb-PAPER-2020-002
 June 5, 2022

Measurement of CP -averaged observables in the $B^0 \rightarrow K^{*0} \mu^+ \mu^-$ decay

LHCb collaboration[†]

Abstract

An angular analysis of the $B^0 \rightarrow K^{*0}(\rightarrow K^+ \pi^-) \mu^+ \mu^-$ decay is presented using a data set corresponding to an integrated luminosity of 4.7 fb^{-1} of pp collision data collected with the LHCb experiment. The full set of CP -averaged observables are determined in bins of the invariant mass squared of the dimuon system. Contamination from decays with the $K^+ \pi^-$ system in an S-wave configuration is taken into account. The tension seen between the previous LHCb results and the Standard Model predictions persists with the new data. The precise value of the significance of this tension depends on the choice of theory nuisance parameters.

Submitted to Phys. Rev. Lett.

© 2022 CERN for the benefit of the LHCb collaboration, license CC BY 4.0 licence.

[†]Authors are listed at the end of this paper.

Decays mediated by the quark-level transition $b \rightarrow s\ell^+\ell^-$, where ℓ represents a lepton, have been the subject of intense recent study, as angular observables [1–8], branching fractions [8–11] and ratios of branching fractions between decays with different flavours of leptons [12–16] have been measured to be in tension with Standard Model (SM) predictions. Such decays are suppressed in the SM, as they proceed only through amplitudes that involve electroweak loop diagrams. The decays are sensitive to virtual contributions from new particles, which could have masses that are inaccessible to direct searches. The observed anomalies with respect to SM predictions can be explained consistently in New Physics models that introduce an additional vector or axial-vector contribution [17–35]. However, there is still considerable debate about whether some of the observations might instead be explained by hadronic uncertainties associated with the transition form factors, or by other long-distance effects [36–39].

The LHCb collaboration presented a measurement of the angular observables of the $B^0 \rightarrow K^{*0}\mu^+\mu^-$ decay in Ref. [1] and found that the data could be explained by modifying the real part of the vector coupling strength of the decays, conventionally denoted $\mathcal{R}e(C_9)$. The analysis used the nuisance parameters from Ref. [40], implemented in the **EOS** software package described in Ref. [41], and found a 3.4 standard deviation (σ) tension with the SM value of $\mathcal{R}e(C_9)$. The tension observed depends on the values of various SM nuisance parameters, including form-factor parameters and subleading corrections used to account for long-distance QCD interference effects with the charmonium modes. Using the **FLAVIO** software package [42], with its default SM nuisance parameters, gives a tension of 3.0σ with respect to the SM value of $\mathcal{R}e(C_9)$ when fitting the angular observables from Ref. [1]. The nuisance parameters include a recent treatment of the subleading corrections [43, 44] that was not available at the time of the previous analysis.

This letter presents the most precise measurements of the complete set of CP -averaged angular observables in the decay $B^0 \rightarrow K^{*0}\mu^+\mu^-$. The data set corresponds to an integrated luminosity of 4.7 fb^{-1} of pp collisions collected with the LHCb experiment. The data were taken in the years 2011, 2012 and 2016, at centre-of-mass energies of 7, 8 and 13 TeV, respectively. The analysis uses the same technique as the analysis described in Ref. [1] but the data sample contains approximately twice as many B^0 decays, owing to the addition of the 2016 data. The same 2011 and 2012 (Run 1) data as in Ref. [1] are used in the present analysis. The results presented in this letter supersede the previous LHCb publication. The combination of the Run 1 data set with the 2016 data set requires a simultaneous angular fit to account for efficiency and reconstruction differences between years. Throughout this letter, K^{*0} is used to refer to the $K^*(892)^0$ resonance and the inclusion of charge-conjugate processes is implied. The K^{*0} meson is reconstructed through the decay $K^{*0} \rightarrow K^+\pi^-$.

The final state of the $B^0 \rightarrow K^{*0}\mu^+\mu^-$ decay can be described by the invariant mass squared of the dimuon system, q^2 , the invariant mass of the $K^+\pi^-$ system, and the three decay angles, $\vec{\Omega} = (\cos\theta_l, \cos\theta_K, \phi)$. The angle between the μ^+ (μ^-) and the direction opposite to that of the B^0 (\bar{B}^0) in the rest frame of the dimuon system is denoted θ_l . The angle between the direction of the K^+ (K^-) and the B^0 (\bar{B}^0) in the rest frame of the K^{*0} (\bar{K}^{*0}) system is denoted θ_K . The angle between the plane defined by the dimuon pair and the plane defined by the kaon and pion in the B^0 (\bar{B}^0) rest frame is denoted ϕ . A full description of the angular basis is provided in Ref. [45].

Following the definitions given in Refs. [1, 46], the CP -averaged angular distribution of the $B^0 \rightarrow K^{*0}\mu^+\mu^-$ decay with the $K^+\pi^-$ system in a P-wave configuration can be

written as

$$\begin{aligned}
\frac{1}{d(\Gamma + \bar{\Gamma})/dq^2} \left. \frac{d^4(\Gamma + \bar{\Gamma})}{dq^2 d\vec{\Omega}} \right|_P = & \frac{9}{32\pi} \left[\frac{3}{4}(1 - F_L) \sin^2 \theta_K + F_L \cos^2 \theta_K \right. \\
& + \frac{1}{4}(1 - F_L) \sin^2 \theta_K \cos 2\theta_l \\
& - F_L \cos^2 \theta_K \cos 2\theta_l + S_3 \sin^2 \theta_K \sin^2 \theta_l \cos 2\phi \\
& + S_4 \sin 2\theta_K \sin 2\theta_l \cos \phi + S_5 \sin 2\theta_K \sin \theta_l \cos \phi \\
& + \frac{4}{3}A_{FB} \sin^2 \theta_K \cos \theta_l + S_7 \sin 2\theta_K \sin \theta_l \sin \phi \\
& \left. + S_8 \sin 2\theta_K \sin 2\theta_l \sin \phi + S_9 \sin^2 \theta_K \sin^2 \theta_l \sin 2\phi \right],
\end{aligned} \tag{1}$$

where F_L is the fraction of the longitudinal polarisation of the K^{*0} meson, A_{FB} is the forward-backward asymmetry of the dimuon system and S_i are other CP -averaged observables [1]. The $K^+\pi^-$ system can also be in an S-wave configuration, which modifies the angular distribution to

$$\begin{aligned}
\frac{1}{d(\Gamma + \bar{\Gamma})/dq^2} \left. \frac{d^4(\Gamma + \bar{\Gamma})}{dq^2 d\vec{\Omega}} \right|_{S+P} = & (1 - F_S) \frac{1}{d(\Gamma + \bar{\Gamma})/dq^2} \left. \frac{d^4(\Gamma + \bar{\Gamma})}{dq^2 d\vec{\Omega}} \right|_P \\
& + \frac{3}{16\pi} F_S \sin^2 \theta_l \\
& + \frac{9}{32\pi} (S_{11} + S_{13} \cos 2\theta_l) \cos \theta_K \\
& + \frac{9}{32\pi} (S_{14} \sin 2\theta_l + S_{15} \sin \theta_l) \sin \theta_K \cos \phi \\
& + \frac{9}{32\pi} (S_{16} \sin \theta_l + S_{17} \sin 2\theta_l) \sin \theta_K \sin \phi,
\end{aligned} \tag{2}$$

where F_S denotes the S-wave fraction and the coefficients S_{11} , S_{13} – S_{17} arise from interference between the S- and P-wave amplitudes. Throughout this letter, F_S and the interference terms between the S- and P-wave are treated as nuisance parameters.

Additional sets of observables, for which the leading $B^0 \rightarrow K^{*0}$ form-factor uncertainties cancel, can be built from F_L , A_{FB} and S_3 – S_9 . Examples of such *optimised* observables include the $P_i^{(\prime)}$ series of observables [47]. The notation used in this letter again follows Ref. [1], for example $P'_5 = S_5 / \sqrt{F_L(1 - F_L)}$.

The LHCb detector is a single-arm forward spectrometer covering the pseudorapidity range $2 < \eta < 5$, described in detail in Refs. [48, 49]. The detector includes a vertex detector surrounding the proton-proton interaction region, tracking stations on either side of a dipole magnet, ring-imaging Cherenkov (RICH) detectors, electromagnetic and hadronic calorimeters and muon chambers.

Simulated signal events are used in this analysis to determine the impact of the detector geometry, trigger, reconstruction and candidate selection on the angular distribution of the signal. The simulation is produced using the software described in Refs. [50–55]. Corrections derived from the data are applied to the simulation to account for mismodelling of the charge multiplicity of the event, B^0 momentum spectrum and B^0 vertex quality. Similarly, the simulated particle identification (PID) performance is corrected to match that determined from control samples selected from the data [56, 57].

The online event selection is performed by a trigger, which comprises a hardware stage, based on information from the calorimeter and muon systems, followed by a software stage that applies a full event reconstruction [58]. Offline, signal candidates are formed from a pair of oppositely charged tracks that are identified as muons, combined with a K^{*0} candidate.

The distribution of the reconstructed $K^+\pi^-\mu^+\mu^-$ invariant mass, $m(K^+\pi^-\mu^+\mu^-)$, is used to discriminate signal from background. This distribution is fitted simultaneously with the three decay angles. The distribution of the reconstructed $K^+\pi^-$ mass, $m(K^+\pi^-)$, depends on the $K^+\pi^-$ angular-momentum configuration and is used to constrain the S-wave fraction. The analysis procedure is cross-checked by performing a fit of the $b \rightarrow c\bar{c}s$ tree-level decay $B^0 \rightarrow J/\psi K^{*0}$, with $J/\psi \rightarrow \mu^+\mu^-$, which results in the same final-state particles. Hereafter, the $B^0 \rightarrow J/\psi(\rightarrow \mu^+\mu^-)K^{*0}$ decay and the equivalent decay via the $\psi(2S)$ resonance are denoted by $B^0 \rightarrow J/\psi K^{*0}$ and $B^0 \rightarrow \psi(2S)K^{*0}$, respectively.

Two types of backgrounds are considered: combinatorial background, where the selected particles do not originate from a single b -hadron decay; and peaking backgrounds, where a single decay is selected but with some of the final-state particles misidentified. The combinatorial background is distributed smoothly in $m(K^+\pi^-\mu^+\mu^-)$, whereas the peaking backgrounds can accumulate in specific regions of the reconstructed mass. In addition, the decays $B^0 \rightarrow J/\psi K^{*0}$, $B^0 \rightarrow \psi(2S)K^{*0}$ and $B^0 \rightarrow \phi(1020)(\rightarrow \mu^+\mu^-)K^{*0}$ are removed by rejecting events with q^2 in the ranges $8.0 < q^2 < 11.0 \text{ GeV}^2/c^4$, $12.5 < q^2 < 15.0 \text{ GeV}^2/c^4$ or $0.98 < q^2 < 1.10 \text{ GeV}^2/c^4$.

The criteria used to select candidates from the Run 1 data are the same as those described in Ref. [1]. The selection of the 2016 data follows closely that of the Run 1 data. Candidates are required to have $5170 < m(K^+\pi^-\mu^+\mu^-) < 5700 \text{ MeV}/c^2$ and $795.9 < m(K^+\pi^-) < 995.9 \text{ MeV}/c^2$. The four tracks of the final-state particles are required to have significant impact parameter (IP) with respect to all primary vertices (PVs) in the event. The tracks are fitted to a common vertex, which is required to be of good quality. The IP of the B^0 candidate is required to be small with respect to one of the PVs. The vertex of the B^0 candidate is required to be significantly displaced from the same PV. The angle between the reconstructed B^0 momentum and the vector connecting this PV to the reconstructed B^0 decay vertex, θ_{DIRA} , is also required to be small. To avoid the same track being used to construct more than one of the final state particles, the opening angle between every pair of tracks is required to be larger than 1 mrad.

Combinatorial background is reduced further using a boosted decision tree (BDT) algorithm [59, 60]. The BDT is trained entirely on data with $B^0 \rightarrow J/\psi K^{*0}$ candidates used as a proxy for the signal and candidates from the upper-mass sideband $5350 < m(K^+\pi^-\mu^+\mu^-) < 7000 \text{ MeV}/c^2$ used as a proxy for the background. The training uses a cross-validation technique [61]. The input variables used are the reconstructed B^0 decay-time and vertex-fit quality, the momentum and transverse momentum of the B^0 candidate, θ_{DIRA} , PID information from the RICH detectors and the muon system, and variables describing the isolation of the final-state tracks [62]. The variables that are used in the BDT are chosen so as to induce the minimum possible distortion in the angular and q^2 distributions. A requirement is placed on the BDT output to maximise the signal significance. This requirement rejects more than 97% of the remaining combinatorial background, while retaining more than 85% of the signal. The signal efficiency of the BDT is uniform in the $m(K^+\pi^-\mu^+\mu^-)$ and $m(K^+\pi^-)$ distributions.

Peaking backgrounds from $B_s^0 \rightarrow \phi(1020)(\rightarrow K^+K^-)\mu^+\mu^-$, $A_b^0 \rightarrow pK^-\mu^+\mu^-$,

$B^0 \rightarrow J/\psi K^{*0}$, $B^0 \rightarrow \psi(2S)K^{*0}$ and $\bar{B}^0 \rightarrow \bar{K}^{*0}\mu^+\mu^-$ decays are considered, where the latter constitutes a background if the kaon from the \bar{K}^{*0} decay is misidentified as the pion and vice versa. In each case, at least one particle needs to be misidentified for the decay to be reconstructed as a signal candidate. Vetoos to reduce these peaking backgrounds are formed by placing requirements on the invariant mass of the candidates, recomputed with the relevant change in the particle mass hypotheses, and by using PID information. In addition, in order to avoid having a strongly peaking contribution to the $\cos \theta_K$ angular distribution in the upper mass sideband, $B^+ \rightarrow K^+\mu^+\mu^-$ candidates with $K^+\mu^+\mu^-$ invariant mass within $60\text{ MeV}/c^2$ of the B^+ mass are removed. The background from b -hadron decays with two hadrons misidentified as muons is negligible. The signal efficiency and residual peaking backgrounds are estimated using simulated events. The vetoes remove a negligible amount of signal. The largest residual backgrounds are from $\bar{B}^0 \rightarrow \bar{K}^{*0}\mu^+\mu^-$, $A_b^0 \rightarrow pK^-\mu^+\mu^-$ and $B_s^0 \rightarrow \phi(1020)(\rightarrow K^+K^-)\mu^+\mu^-$ decays, at the level of 1% or less of the expected signal yield. This is sufficiently small such that these backgrounds are neglected in the angular analysis and are considered only as sources of systematic uncertainty.

A simultaneous fit to the Run 1 data and the 2016 data is performed, with the angular observables as common fit parameters. For each data set, an unbinned maximum-likelihood fit to the distributions of $m(K^+\pi^-\mu^+\mu^-)$ and the three decay angles is used to determine the CP -averaged angular observables in bins of q^2 , in either the standard or optimised basis; and a simultaneous fit of the $m(K^+\pi^-)$ invariant mass distribution is used to constrain the S-wave fraction. The fitted probability density functions (PDFs) are of an identical form to those of Ref. [1], as are the q^2 bins used. In addition to the narrow q^2 bins, results are obtained for the wider bins $1.1 < q^2 < 6.0\text{ GeV}^2/c^4$ and $15.0 < q^2 < 19.0\text{ GeV}^2/c^4$.

The angular distribution of the signal is described using Eq. (1). The $P_i^{(\prime)}$ observables are determined by reparameterising Eq. (1) using a basis comprising F_L , $P_{1,2,3}$ and $P'_{4,5,6,8}$. The angular distribution is multiplied by an acceptance model used to account for the effect of the reconstruction and candidate selection. The acceptance function is parameterised in four dimensions, according to

$$\varepsilon(\cos \theta_l, \cos \theta_K, \phi, q^2) = \sum_{ijmn} c_{ijmn} L_i(\cos \theta_l) L_j(\cos \theta_K) L_m(\phi) L_n(q^2), \quad (3)$$

where the terms $L_h(x)$ denote Legendre polynomials of order h and the values of the angles and q^2 are rescaled to the range $-1 < x < +1$ when evaluating the polynomials. For the $\cos \theta_l$, $\cos \theta_K$ and ϕ angles, the sum in Eq. (3) encompasses $L_h(x)$ up to fourth, fifth and sixth order, respectively. The q^2 parameterisation comprises $L_h(x)$ up to fifth order. Simulation indicates that the acceptance function can be assumed to be flat across $m(K^+\pi^-)$. The coefficients c_{ijmn} are determined using a principal moment analysis of simulated $B^0 \rightarrow K^{*0}\mu^+\mu^-$ decays. As all of the relevant kinematic variables needed to describe the decay are used in this parameterisation, the acceptance function does not depend on the decay model used in the simulation.

In the narrow q^2 bins, the acceptance is taken to be constant across each bin and is included in the fit by multiplying Eq. (2) by the acceptance function evaluated with the value of q^2 fixed at the bin centre. In the wider q^2 bins, the shape of the acceptance can vary significantly across the bin. In the likelihood, candidates are therefore weighted by the inverse of the acceptance function and parameter uncertainties are obtained using a bootstrapping technique [63].

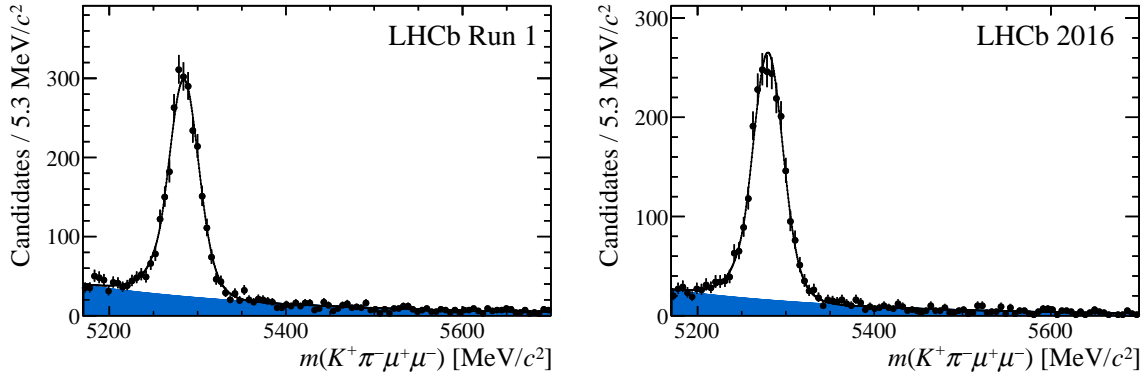


Figure 1: The $K^+\pi^-\mu^+\mu^-$ mass distribution of candidates with $0.1 < q^2 < 19.0 \text{ GeV}^2/c^4$, excluding the $\phi(1020)$ and charmonium regions, for the (left) Run 1 data and (right) 2016 data. The background is indicated by the shaded region.

The background angular distribution is modelled with second-order polynomials in $\cos\theta_l$, $\cos\theta_K$ and ϕ , with the angular coefficients allowed to vary in the fit. This angular distribution is assumed to factorise in the three decay angles, which is confirmed to be the case for candidates in the upper mass sideband of the data.

The $m(K^+\pi^-\mu^+\mu^-)$ distribution of the signal candidates is modelled using the sum of two Gaussian functions with a common mean, each with a power-law tail on the low mass side. The parameters describing the signal mass shape are determined from a fit to the $B^0 \rightarrow J/\psi K^{*0}$ decay in the data and are subsequently fixed when fitting the $B^0 \rightarrow K^{*0}\mu^+\mu^-$ candidates. For each of the q^2 bins, a scale factor that is determined from simulation is included to account for the difference in resolution between the $B^0 \rightarrow J/\psi K^{*0}$ and $B^0 \rightarrow K^{*0}\mu^+\mu^-$ decay modes. A component is included in the $B^0 \rightarrow J/\psi K^{*0}$ fit to account for $\bar{B}_s^0 \rightarrow J/\psi K^{*0}$ decays, which are at the level of $\sim 1\%$ of the $B^0 \rightarrow J/\psi K^{*0}$ signal yield. The background from the equivalent Cabibbo-suppressed penguin decay, $\bar{B}_s^0 \rightarrow K^{*0}\mu^+\mu^-$ [64], is negligible and is ignored in the fit of the signal decay. The combinatorial background is described well by an exponential distribution in $m(K^+\pi^-\mu^+\mu^-)$.

The K^{*0} signal component in the $m(K^+\pi^-)$ distribution is modelled using a relativistic Breit-Wigner function for the P-wave component and the LASS parameterisation [65] for the S-wave component. The combinatorial background is described by a linear function in $m(K^+\pi^-)$.

The decay $B^0 \rightarrow J/\psi K^{*0}$ is used to cross-check the analysis procedure in the region $8.0 < q^2 < 11.0 \text{ GeV}^2/c^4$. This decay is selected in the data with negligible background contamination. The angular structure has been determined by measurements made by the BaBar, Belle and LHCb collaborations [66–68]. The $B^0 \rightarrow J/\psi K^{*0}$ angular observables obtained from the Run 1 and 2016 LHCb data, using the acceptance correction derived as described above, are in good agreement with these previous measurements.

Figure 1 shows the projection of the fitted PDF on the $K^+\pi^-\mu^+\mu^-$ mass distribution. The $B^0 \rightarrow K^{*0}\mu^+\mu^-$ yield, integrated over the q^2 ranges $0.10 < q^2 < 0.98 \text{ GeV}^2/c^4$, $1.1 < q^2 < 8.0 \text{ GeV}^2/c^4$, $11.0 < q^2 < 12.5 \text{ GeV}^2/c^4$ and $15.0 < q^2 < 19.0 \text{ GeV}^2/c^4$, is determined to be 2398 ± 57 for the Run 1 data, and 2187 ± 53 for the 2016 data.

Pseudoexperiments, generated using the results of the best fit to data, are used to assess the bias and coverage of the fit. The majority of observables have a bias of less than

10% of their statistical uncertainty, with the largest bias being 17%, and all observables have an uncertainty estimate within 10% of the true uncertainty. The biases are driven by boundary effects in the observables. The largest effect comes from requiring that $F_S \geq 0$, which can bias F_S to larger values. This can then result in a bias in the P-wave observables (see Eq. 2). The statistical uncertainty is corrected to account for any under- or over-coverage and a systematic uncertainty equal to the size of the observed bias is assigned.

The size of other sources of systematic uncertainty is estimated using pseudoexperiments, in which one or more parameters are varied and the angular observables are determined with and without this variation. The systematic uncertainty is then taken as the average of the difference between the two models. The pseudoexperiments are generated with signal yields many times larger than the data, in order to render statistical fluctuations negligible.

The size of the total systematic uncertainty varies depending on the angular observable and the q^2 bin. The majority of observables in both the S_i and $P_i^{(\prime)}$ basis have a total systematic uncertainty between 5% and 25% of the statistical uncertainty. For F_L , the systematic uncertainty tends to be larger, typically between 20% and 50%. The systematic uncertainties are given in Table 3 of the Supplemental Material.

The dominant systematic uncertainties arise from the peaking backgrounds that are neglected in the analysis, the bias correction, and, for the narrow q^2 bins, from the uncertainty associated with evaluating the acceptance at a fixed point in q^2 . For the peaking backgrounds, the systematic uncertainty is evaluated by injecting additional candidates, drawn from the angular distributions of the background modes, into the pseudoexperiment data. The systematic uncertainty for the bias correction is determined directly from the pseudoexperiments used to validate the fit. The systematic uncertainty from the variation of the acceptance with q^2 is determined by moving the point in q^2 at which the acceptance is evaluated to halfway between the bin centre and the upper and the lower edge. The largest deviation is taken as the systematic uncertainty. Examples of further sources of systematic uncertainty investigated include the $m(K^+\pi^-)$ lineshape for the S-wave contribution, the assumption that the acceptance function is flat across the $m(K^+\pi^-)$ mass, and the effect of the $B^+ \rightarrow K^+\mu^+\mu^-$ veto on the angular distribution of the background. These sources make a negligible contribution to the total uncertainty. With respect to the analysis of Ref. [1], the systematic uncertainty from residual differences between data and simulation is significantly reduced, owing to an improved decay model for $B^0 \rightarrow J/\psi K^{*0}$ decays [67].

The CP -averaged observables F_L , A_{FB} , S_5 and P'_5 that are obtained from the S_i and $P_i^{(\prime)}$ fits are shown together with their respective SM predictions in Fig. 2. The results for all observables are given in Figs. 3 and 4 and Tables 1 and 2 of the Supplemental Material. In addition, the statistical correlation between the observables is provided in Tables 4–23. The SM predictions are based on the prescription of Ref. [44], which combines light-cone sum rule calculations [43], valid in the low- q^2 region, with lattice determinations at high q^2 [71, 72] to yield more precise determinations of the form factors over the full q^2 range. For the $P_i^{(\prime)}$ observables, predictions from Ref. [69] are shown using form factors from Ref. [70]. These predictions are restricted to the region $q^2 < 8.0 \text{ GeV}^2/c^4$. The results from Run 1 and the 2016 data are in excellent agreement. A stand-alone fit to the Run 1 data reproduces exactly the central values of the observables obtained in Ref. [1].

Considering the observables individually, the results are largely in agreement with the

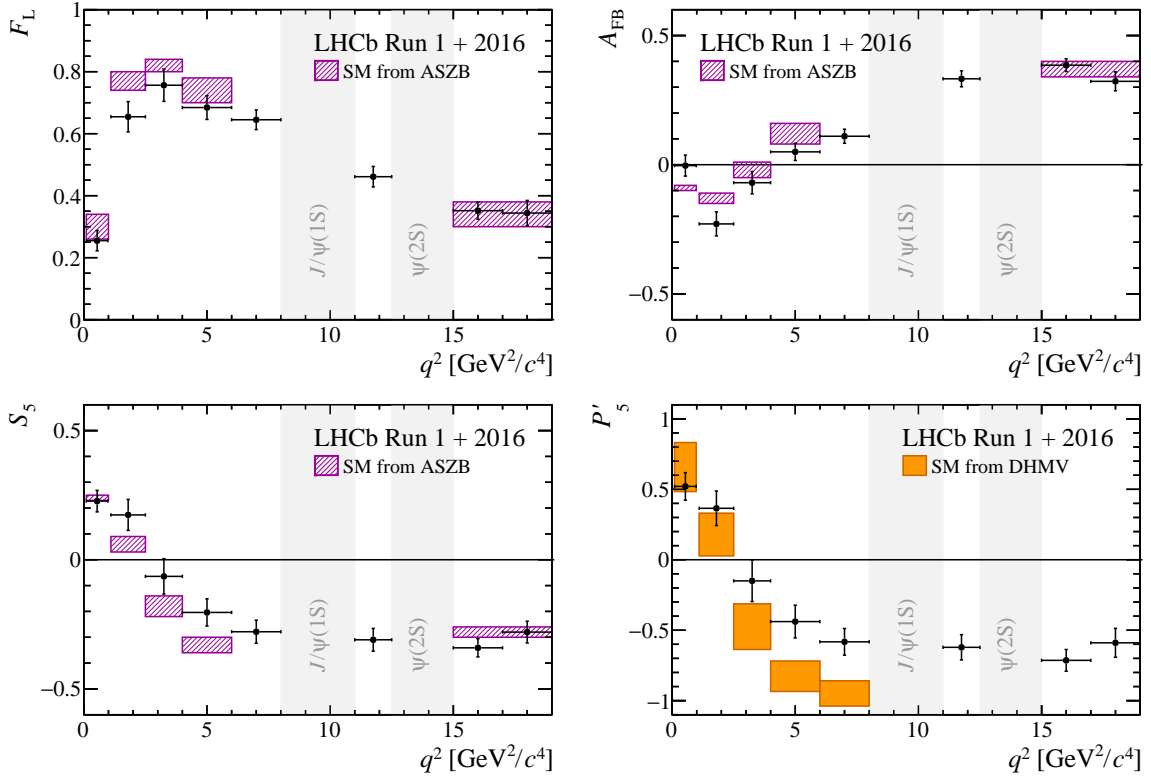


Figure 2: Results for the CP -averaged angular observables F_L , A_{FB} , S_5 and P'_5 in bins of q^2 . The data are compared to SM predictions based on the prescription of Refs. [43, 44], with the exception of the P'_5 distribution, which is compared to SM predictions based on Refs. [69, 70].

SM predictions. The local discrepancy in the P'_5 observable in the $4.0 < q^2 < 6.0 \text{ GeV}^2/c^4$ and $6.0 < q^2 < 8.0 \text{ GeV}^2/c^4$ bins reduces from the 2.8 and 3.0σ observed in Ref. [1] to 2.5 and 2.9σ . However, as discussed below, the overall tension with the SM is observed to increase mildly.

Using the FLAVIO software package [42], a fit of the angular observables is performed varying the parameter $\mathcal{R}e(C_9)$. The default FLAVIO SM nuisance parameters are used, including form-factor parameters and subleading corrections to account for long-distance QCD interference effects with the charmonium decay modes [43, 44]. The same q^2 bins as in Ref. [1] are included. The 3.0σ discrepancy with respect to the SM value of $\mathcal{R}e(C_9)$ obtained with the Ref. [1] data set changes to 3.3σ with the data set used here. The best fit to the angular distribution is obtained with a shift in the SM value of $\mathcal{R}e(C_9)$ by $-0.99^{+0.25}_{-0.21}$. The tension observed in any such fit will depend on the effective coupling(s) varied, the handling of the SM nuisance parameters and the q^2 bins that are included in the fit. For example, the $6.0 < q^2 < 8.0 \text{ GeV}^2/c^4$ bin is known to be associated with larger theoretical uncertainties [46]. Neglecting this bin, a FLAVIO fit gives a tension of 2.4σ using the observables from Ref. [1] and 2.7σ tension with the measurements reported here.

In summary, using 4.7 fb^{-1} of pp collision data collected with the LHCb experiment during the years 2011, 2012 and 2016, a complete set of CP -averaged angular observables has been measured for the $B^0 \rightarrow K^{*0}\mu^+\mu^-$ decay. These are the most precise measurements of these quantities to date.

Acknowledgements

We express our gratitude to our colleagues in the CERN accelerator departments for the excellent performance of the LHC. We thank the technical and administrative staff at the LHCb institutes. We acknowledge support from CERN and from the national agencies: CAPES, CNPq, FAPERJ and FINEP (Brazil); MOST and NSFC (China); CNRS/IN2P3 (France); BMBF, DFG and MPG (Germany); INFN (Italy); NWO (The Netherlands); MNiSW and NCN (Poland); MEN/IFA (Romania); MinES and FASO (Russia); MinECo (Spain); SNSF and SER (Switzerland); NASU (Ukraine); STFC (United Kingdom); NSF (USA). We acknowledge the computing resources that are provided by CERN, IN2P3 (France), KIT and DESY (Germany), INFN (Italy), SURF (The Netherlands), PIC (Spain), GridPP (United Kingdom), RRCKI and Yandex LLC (Russia), CSCS (Switzerland), IFIN-HH (Romania), CBPF (Brazil), PL-GRID (Poland) and OSC (USA). We are indebted to the communities behind the multiple open source software packages on which we depend. Individual groups or members have received support from AvH Foundation (Germany), EPLANET, Marie Skłodowska-Curie Actions and ERC (European Union), Conseil Général de Haute-Savoie, Labex ENIGMASS and OCEVU, Région Auvergne (France), RFBR and Yandex LLC (Russia), GVA, XuntaGal and GENCAT (Spain), Herchel Smith Fund, The Royal Society, Royal Commission for the Exhibition of 1851 and the Leverhulme Trust (United Kingdom).

Supplemental Material

This supplemental material includes additional information to that already provided in the main letter. A full set of results for the nominal analysis is presented in both graphical and tabular form in Sec. 1. A complete description of the corresponding systematic uncertainties is given in Sec. 2. The correlations between the angular observables are presented for the S_i observables in Sec. 3 and for the $P_i^{(l)}$ observables in Sec. 4. The angular and mass distributions of the selected candidates in the different q^2 bins are shown in Sec. 5.

1 Results

The values of S_3 , S_4 and S_7 – S_9 obtained from the simultaneous fit are shown in Fig. 3. The data are compared to theoretical predictions based on the prescription of Ref. [44]. The predictions combine light-cone sum rule calculations [43] with lattice determinations [71,72] of the $B^0 \rightarrow K^{*0}$ form factors. Figure 4 shows the values of the optimised observables, $P_i^{(l)}$, obtained from the fit. The data are compared to predictions based on the prescription in Ref. [69]. These predictions use form factors from Ref. [70]. The values of the observables in the standard and optimised basis are given in Tables 1 and 2, respectively. The statistical correlation between the observables in each q^2 bin is provided in Tables 4–13 and Tables 14–23.

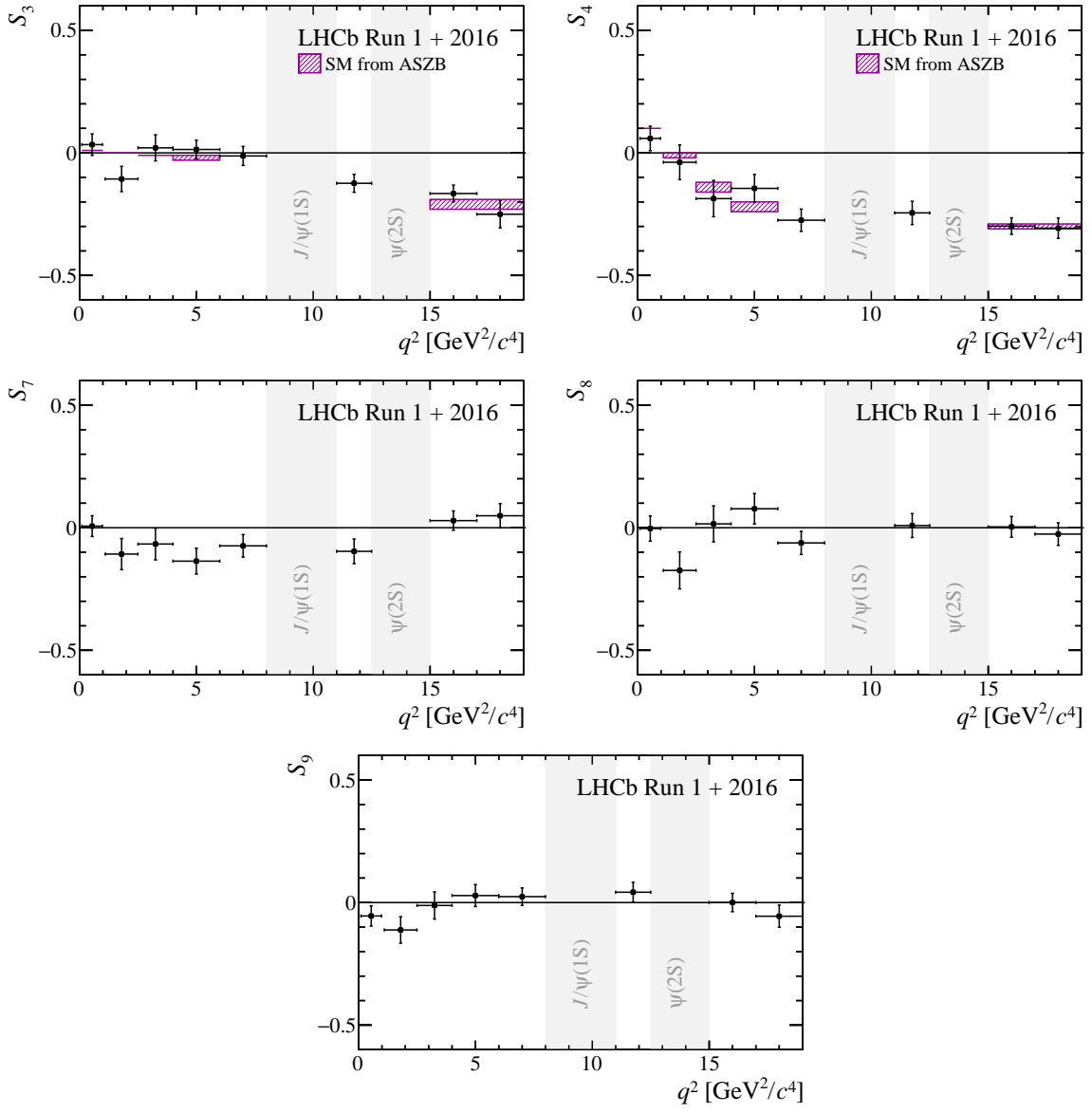


Figure 3: Results for the CP -averaged angular observables S_3 , S_4 and S_7 – S_9 in bins of q^2 . The data are compared to SM predictions based on the prescription of Refs. [43, 44].

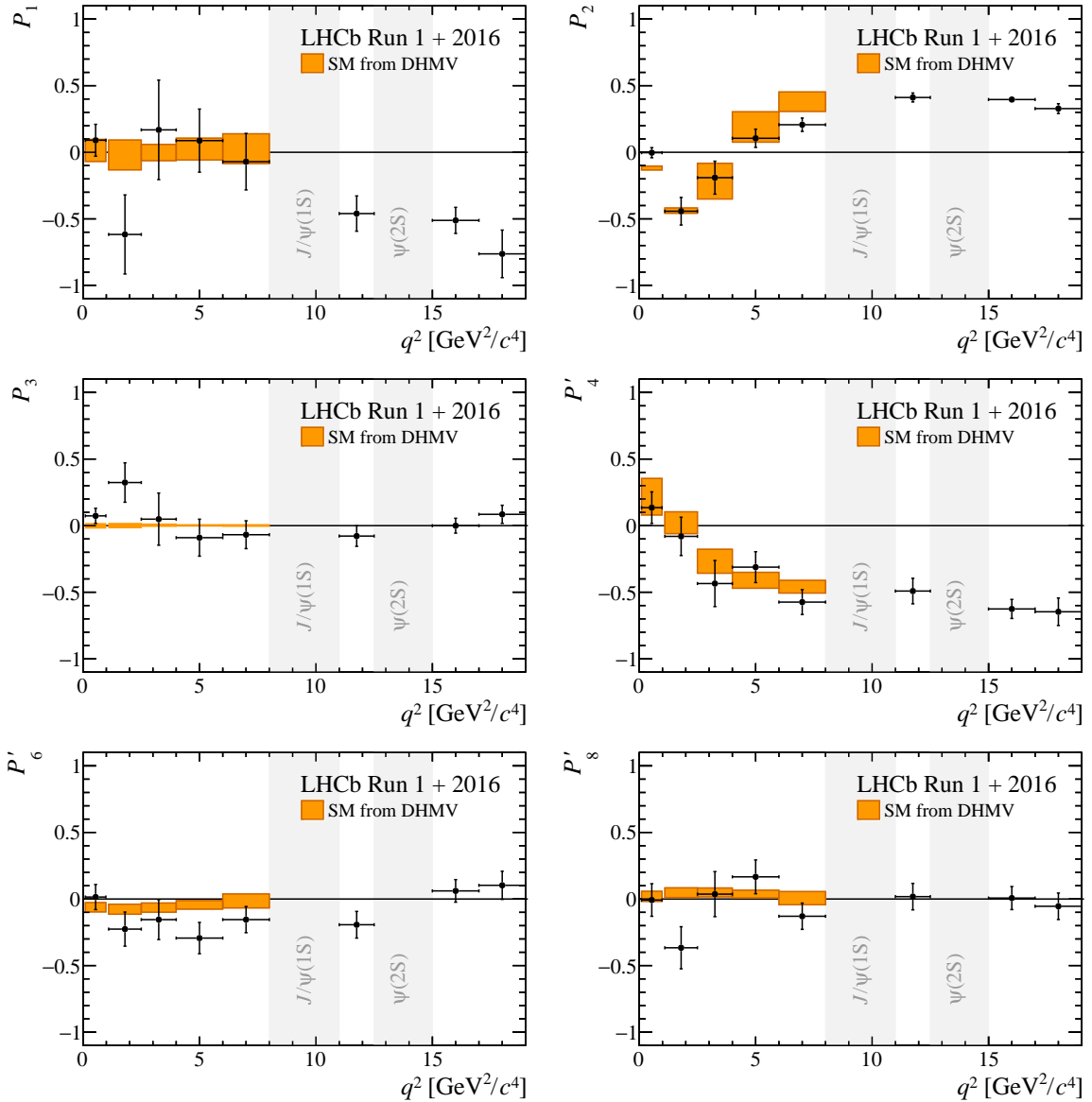


Figure 4: Results for the optimised angular observables P_1 – P_3 , P'_4 , P'_6 and P'_8 in bins of q^2 . The data are compared to SM predictions based on Refs. [69, 70].

Table 1: Results for the CP -averaged observables F_L , A_{FB} and S_3 – S_9 . The first uncertainties are statistical and the second systematic.

$0.10 < q^2 < 0.98 \text{ GeV}^2/c^4$		$1.1 < q^2 < 2.5 \text{ GeV}^2/c^4$		$2.5 < q^2 < 4.0 \text{ GeV}^2/c^4$	
F_L	$0.255 \pm 0.032 \pm 0.007$	F_L	$0.655 \pm 0.046 \pm 0.017$	F_L	$0.756 \pm 0.047 \pm 0.023$
S_3	$0.034 \pm 0.044 \pm 0.003$	S_3	$-0.107 \pm 0.052 \pm 0.003$	S_3	$0.020 \pm 0.053 \pm 0.002$
S_4	$0.059 \pm 0.050 \pm 0.004$	S_4	$-0.038 \pm 0.070 \pm 0.011$	S_4	$-0.187 \pm 0.074 \pm 0.008$
S_5	$0.227 \pm 0.041 \pm 0.008$	S_5	$0.174 \pm 0.060 \pm 0.007$	S_5	$-0.064 \pm 0.068 \pm 0.010$
A_{FB}	$-0.004 \pm 0.040 \pm 0.004$	A_{FB}	$-0.229 \pm 0.046 \pm 0.009$	A_{FB}	$-0.070 \pm 0.043 \pm 0.006$
S_7	$0.006 \pm 0.042 \pm 0.002$	S_7	$-0.107 \pm 0.063 \pm 0.004$	S_7	$-0.066 \pm 0.065 \pm 0.004$
S_8	$-0.003 \pm 0.051 \pm 0.001$	S_8	$-0.174 \pm 0.075 \pm 0.002$	S_8	$0.016 \pm 0.074 \pm 0.002$
S_9	$-0.055 \pm 0.041 \pm 0.002$	S_9	$-0.112 \pm 0.054 \pm 0.005$	S_9	$-0.012 \pm 0.055 \pm 0.003$
$4.0 < q^2 < 6.0 \text{ GeV}^2/c^4$		$6.0 < q^2 < 8.0 \text{ GeV}^2/c^4$		$11.0 < q^2 < 12.5 \text{ GeV}^2/c^4$	
F_L	$0.684 \pm 0.035 \pm 0.015$	F_L	$0.645 \pm 0.030 \pm 0.011$	F_L	$0.461 \pm 0.031 \pm 0.010$
S_3	$0.014 \pm 0.038 \pm 0.003$	S_3	$-0.013 \pm 0.038 \pm 0.004$	S_3	$-0.124 \pm 0.037 \pm 0.003$
S_4	$-0.145 \pm 0.057 \pm 0.004$	S_4	$-0.275 \pm 0.045 \pm 0.006$	S_4	$-0.245 \pm 0.047 \pm 0.007$
S_5	$-0.204 \pm 0.051 \pm 0.013$	S_5	$-0.279 \pm 0.043 \pm 0.013$	S_5	$-0.310 \pm 0.043 \pm 0.011$
A_{FB}	$0.050 \pm 0.033 \pm 0.002$	A_{FB}	$0.110 \pm 0.027 \pm 0.005$	A_{FB}	$0.333 \pm 0.030 \pm 0.008$
S_7	$-0.136 \pm 0.053 \pm 0.002$	S_7	$-0.074 \pm 0.046 \pm 0.003$	S_7	$-0.096 \pm 0.050 \pm 0.003$
S_8	$0.077 \pm 0.062 \pm 0.001$	S_8	$-0.062 \pm 0.047 \pm 0.001$	S_8	$0.009 \pm 0.049 \pm 0.001$
S_9	$0.029 \pm 0.045 \pm 0.002$	S_9	$0.024 \pm 0.035 \pm 0.002$	S_9	$0.042 \pm 0.040 \pm 0.003$
$15.0 < q^2 < 17.0 \text{ GeV}^2/c^4$		$17.0 < q^2 < 19.0 \text{ GeV}^2/c^4$		$1.1 < q^2 < 6.0 \text{ GeV}^2/c^4$	
F_L	$0.352 \pm 0.026 \pm 0.009$	F_L	$0.344 \pm 0.032 \pm 0.025$	F_L	$0.700 \pm 0.025 \pm 0.013$
S_3	$-0.166 \pm 0.034 \pm 0.007$	S_3	$-0.250 \pm 0.050 \pm 0.025$	S_3	$-0.012 \pm 0.025 \pm 0.003$
S_4	$-0.299 \pm 0.033 \pm 0.008$	S_4	$-0.307 \pm 0.041 \pm 0.008$	S_4	$-0.136 \pm 0.039 \pm 0.003$
S_5	$-0.341 \pm 0.034 \pm 0.009$	S_5	$-0.280 \pm 0.040 \pm 0.014$	S_5	$-0.052 \pm 0.034 \pm 0.007$
A_{FB}	$0.385 \pm 0.024 \pm 0.007$	A_{FB}	$0.323 \pm 0.032 \pm 0.019$	A_{FB}	$-0.073 \pm 0.021 \pm 0.002$
S_7	$0.029 \pm 0.039 \pm 0.001$	S_7	$0.049 \pm 0.049 \pm 0.007$	S_7	$-0.090 \pm 0.034 \pm 0.002$
S_8	$0.003 \pm 0.042 \pm 0.002$	S_8	$-0.026 \pm 0.046 \pm 0.002$	S_8	$-0.009 \pm 0.037 \pm 0.002$
S_9	$0.000 \pm 0.037 \pm 0.002$	S_9	$-0.056 \pm 0.045 \pm 0.002$	S_9	$-0.025 \pm 0.026 \pm 0.002$
$15.0 < q^2 < 19.0 \text{ GeV}^2/c^4$					
F_L	$0.345 \pm 0.020 \pm 0.007$				
S_3	$-0.189 \pm 0.030 \pm 0.009$				
S_4	$-0.303 \pm 0.024 \pm 0.008$				
S_5	$-0.317 \pm 0.024 \pm 0.011$				
A_{FB}	$0.353 \pm 0.020 \pm 0.010$				
S_7	$0.035 \pm 0.030 \pm 0.003$				
S_8	$0.005 \pm 0.031 \pm 0.001$				
S_9	$-0.031 \pm 0.029 \pm 0.001$				

Table 2: Results for the optimised observables $P_i^{(\prime)}$. The first uncertainties are statistical and the second systematic.

$0.10 < q^2 < 0.98 \text{ GeV}^2/c^4$	$1.1 < q^2 < 2.5 \text{ GeV}^2/c^4$	$2.5 < q^2 < 4.0 \text{ GeV}^2/c^4$
P_1 $0.090 \pm 0.119 \pm 0.009$	P_1 $-0.617 \pm 0.296 \pm 0.023$	P_1 $0.168 \pm 0.371 \pm 0.043$
P_2 $-0.003 \pm 0.038 \pm 0.003$	P_2 $-0.443 \pm 0.100 \pm 0.027$	P_2 $-0.191 \pm 0.116 \pm 0.043$
P_3 $0.073 \pm 0.057 \pm 0.003$	P_3 $0.324 \pm 0.147 \pm 0.014$	P_3 $0.049 \pm 0.195 \pm 0.014$
P'_4 $0.135 \pm 0.118 \pm 0.010$	P'_4 $-0.080 \pm 0.142 \pm 0.019$	P'_4 $-0.435 \pm 0.169 \pm 0.035$
P'_5 $0.521 \pm 0.095 \pm 0.024$	P'_5 $0.365 \pm 0.122 \pm 0.013$	P'_5 $-0.150 \pm 0.144 \pm 0.032$
P'_6 $0.015 \pm 0.094 \pm 0.007$	P'_6 $-0.226 \pm 0.128 \pm 0.005$	P'_6 $-0.155 \pm 0.148 \pm 0.024$
P'_8 $-0.007 \pm 0.122 \pm 0.002$	P'_8 $-0.366 \pm 0.158 \pm 0.005$	P'_8 $0.037 \pm 0.169 \pm 0.007$
$4.0 < q^2 < 6.0 \text{ GeV}^2/c^4$	$6.0 < q^2 < 8.0 \text{ GeV}^2/c^4$	$11.0 < q^2 < 12.5 \text{ GeV}^2/c^4$
P_1 $0.088 \pm 0.235 \pm 0.029$	P_1 $-0.071 \pm 0.211 \pm 0.020$	P_1 $-0.460 \pm 0.132 \pm 0.015$
P_2 $0.105 \pm 0.068 \pm 0.009$	P_2 $0.207 \pm 0.048 \pm 0.013$	P_2 $0.411 \pm 0.033 \pm 0.008$
P_3 $-0.090 \pm 0.139 \pm 0.006$	P_3 $-0.068 \pm 0.104 \pm 0.007$	P_3 $-0.078 \pm 0.077 \pm 0.007$
P'_4 $-0.312 \pm 0.115 \pm 0.013$	P'_4 $-0.574 \pm 0.091 \pm 0.018$	P'_4 $-0.491 \pm 0.095 \pm 0.013$
P'_5 $-0.439 \pm 0.111 \pm 0.036$	P'_5 $-0.583 \pm 0.090 \pm 0.030$	P'_5 $-0.622 \pm 0.088 \pm 0.017$
P'_6 $-0.293 \pm 0.117 \pm 0.004$	P'_6 $-0.155 \pm 0.098 \pm 0.009$	P'_6 $-0.193 \pm 0.100 \pm 0.003$
P'_8 $0.166 \pm 0.127 \pm 0.004$	P'_8 $-0.129 \pm 0.098 \pm 0.005$	P'_8 $0.018 \pm 0.099 \pm 0.009$
$15.0 < q^2 < 17.0 \text{ GeV}^2/c^4$	$17.0 < q^2 < 19.0 \text{ GeV}^2/c^4$	$1.1 < q^2 < 6.0 \text{ GeV}^2/c^4$
P_1 $-0.511 \pm 0.096 \pm 0.020$	P_1 $-0.763 \pm 0.152 \pm 0.094$	P_1 $-0.079 \pm 0.159 \pm 0.021$
P_2 $0.396 \pm 0.022 \pm 0.004$	P_2 $0.328 \pm 0.032 \pm 0.017$	P_2 $-0.162 \pm 0.050 \pm 0.012$
P_3 $-0.000 \pm 0.056 \pm 0.003$	P_3 $0.085 \pm 0.068 \pm 0.004$	P_3 $0.085 \pm 0.090 \pm 0.005$
P'_4 $-0.626 \pm 0.069 \pm 0.018$	P'_4 $-0.647 \pm 0.086 \pm 0.057$	P'_4 $-0.298 \pm 0.087 \pm 0.016$
P'_5 $-0.714 \pm 0.074 \pm 0.021$	P'_5 $-0.590 \pm 0.084 \pm 0.059$	P'_5 $-0.114 \pm 0.068 \pm 0.026$
P'_6 $0.061 \pm 0.085 \pm 0.003$	P'_6 $0.103 \pm 0.105 \pm 0.016$	P'_6 $-0.197 \pm 0.075 \pm 0.009$
P'_8 $0.007 \pm 0.086 \pm 0.002$	P'_8 $-0.055 \pm 0.099 \pm 0.006$	P'_8 $-0.020 \pm 0.089 \pm 0.009$
$15.0 < q^2 < 19.0 \text{ GeV}^2/c^4$		
P_1 $-0.577 \pm 0.090 \pm 0.031$		
P_2 $0.359 \pm 0.018 \pm 0.009$		
P_3 $0.048 \pm 0.045 \pm 0.002$		
P'_4 $-0.638 \pm 0.055 \pm 0.020$		
P'_5 $-0.667 \pm 0.053 \pm 0.029$		
P'_6 $0.073 \pm 0.067 \pm 0.006$		
P'_8 $0.011 \pm 0.069 \pm 0.003$		

2 Systematic uncertainties

A summary of the sources of systematic uncertainty on the angular observables is shown in Table 3. Details of how the systematic uncertainties are estimated are given in the letter. The dominant systematic uncertainties arise from the peaking backgrounds that are neglected in the analysis (*peaking backgrounds* in Table 3) and, for the narrow q^2 bins, from the uncertainty associated with evaluating the acceptance at a fixed point in q^2 (*acceptance variation with q^2* in Table 3). The *bias correction* in Table 3 refers to the biases observed when generating pseudoexperiments using the result of the best fit to data, as discussed in the letter.

Table 3: Summary of the different sources of systematic uncertainty on the angular observables.

Source	F_L	A_{FB}, S_3-S_9	$P_1-P'_8$
Acceptance stat. uncertainty	< 0.01	< 0.01	< 0.01
Acceptance polynomial order	< 0.01	< 0.01	< 0.02
Data-simulation differences	< 0.01	< 0.01	< 0.01
Acceptance variation with q^2	< 0.03	< 0.01	< 0.09
$m(K^+\pi^-)$ model	< 0.01	< 0.01	< 0.01
Background model	< 0.01	< 0.01	< 0.02
Peaking backgrounds	< 0.01	< 0.02	< 0.03
$m(K^+\pi^-\mu^+\mu^-)$ model	< 0.01	< 0.01	< 0.01
$K^+\mu^+\mu^-$ veto	< 0.01	< 0.01	< 0.01
Trigger	< 0.01	< 0.01	< 0.01
Bias correction	< 0.02	< 0.01	< 0.03

3 Correlation matrices for the CP -averaged observables

Correlation matrices between the CP -averaged observables in the different q^2 bins are provided in Tables 4–13.

Table 4: Correlation matrix for the CP -averaged observables from the maximum-likelihood fit in the bin $0.10 < q^2 < 0.98 \text{ GeV}^2/c^4$.

	F_L	S_3	S_4	S_5	A_{FB}	S_7	S_8	S_9
F_L	1.00	-0.00	-0.03	0.09	0.03	-0.01	0.06	0.03
S_3		1.00	0.02	0.14	0.02	-0.06	0.01	-0.01
S_4			1.00	0.06	0.15	-0.03	0.06	0.00
S_5				1.00	0.04	-0.03	-0.01	0.00
A_{FB}					1.00	-0.02	-0.01	-0.02
S_7						1.00	-0.04	0.10
S_8							1.00	0.02
S_9								1.00

Table 5: Correlation matrix for the CP -averaged observables from the maximum-likelihood fit in the bin $1.1 < q^2 < 2.5 \text{ GeV}^2/c^4$.

	F_L	S_3	S_4	S_5	A_{FB}	S_7	S_8	S_9
F_L	1.00	0.05	0.04	0.16	0.11	-0.08	-0.06	0.05
S_3		1.00	0.00	0.04	0.05	0.08	0.08	0.18
S_4			1.00	-0.20	-0.01	0.02	-0.09	-0.07
S_5				1.00	-0.09	-0.11	-0.02	-0.12
A_{FB}					1.00	-0.03	0.08	-0.04
S_7						1.00	-0.16	0.14
S_8							1.00	-0.04
S_9								1.00

Table 6: Correlation matrix for the CP -averaged observables from the maximum-likelihood fit in the bin $2.5 < q^2 < 4.0 \text{ GeV}^2/c^4$.

	F_L	S_3	S_4	S_5	A_{FB}	S_7	S_8	S_9
F_L	1.00	-0.02	-0.03	-0.02	-0.03	-0.01	-0.08	0.06
S_3		1.00	-0.05	-0.03	0.05	0.02	-0.07	0.02
S_4			1.00	-0.13	-0.10	0.01	0.03	-0.03
S_5				1.00	-0.08	0.01	0.02	0.03
A_{FB}					1.00	0.06	-0.05	-0.08
S_7						1.00	0.01	0.03
S_8							1.00	-0.08
S_9								1.00

Table 7: Correlation matrix for the CP -averaged observables from the maximum-likelihood fit in the bin $4.0 < q^2 < 6.0 \text{ GeV}^2/c^4$.

	F_L	S_3	S_4	S_5	A_{FB}	S_7	S_8	S_9
F_L	1.00	-0.01	0.05	-0.02	-0.14	-0.10	0.09	0.04
S_3		1.00	-0.06	-0.10	0.06	-0.02	0.02	-0.08
S_4			1.00	0.01	-0.14	0.03	0.02	0.01
S_5				1.00	-0.08	0.07	0.02	-0.05
A_{FB}					1.00	-0.01	-0.03	0.01
S_7						1.00	0.03	-0.18
S_8							1.00	-0.00
S_9								1.00

Table 8: Correlation matrix for the CP -averaged observables from the maximum-likelihood fit in the bin $6.0 < q^2 < 8.0 \text{ GeV}^2/c^4$.

	F_L	S_3	S_4	S_5	A_{FB}	S_7	S_8	S_9
F_L	1.00	0.00	-0.01	-0.06	-0.20	-0.05	0.00	-0.06
S_3		1.00	-0.12	-0.24	0.01	0.05	0.04	-0.10
S_4			1.00	0.13	-0.10	0.02	-0.04	-0.04
S_5				1.00	-0.16	-0.01	0.02	-0.06
A_{FB}					1.00	-0.03	0.02	0.02
S_7						1.00	0.08	-0.09
S_8							1.00	-0.08
S_9								1.00

Table 9: Correlation matrix for the CP -averaged observables from the maximum-likelihood fit in the bin $11.0 < q^2 < 12.5 \text{ GeV}^2/c^4$.

	F_L	S_3	S_4	S_5	A_{FB}	S_7	S_8	S_9
F_L	1.00	0.14	0.02	-0.09	-0.56	0.02	0.01	0.01
S_3		1.00	0.08	-0.08	-0.15	0.02	0.06	-0.10
S_4			1.00	0.08	-0.12	0.03	-0.02	-0.02
S_5				1.00	-0.13	0.03	-0.00	-0.17
A_{FB}					1.00	-0.05	-0.10	0.12
S_7						1.00	0.27	-0.10
S_8							1.00	-0.01
S_9								1.00

Table 10: Correlation matrix for the CP -averaged observables from the maximum-likelihood fit in the bin $15.0 < q^2 < 17.0 \text{ GeV}^2/c^4$.

	F_L	S_3	S_4	S_5	A_{FB}	S_7	S_8	S_9
F_L	1.00	0.27	0.02	0.07	-0.53	0.00	-0.04	0.06
S_3		1.00	-0.05	0.01	-0.12	-0.02	-0.04	0.10
S_4			1.00	0.29	-0.15	0.02	0.06	0.03
S_5				1.00	-0.28	0.06	0.03	0.04
A_{FB}					1.00	0.01	-0.00	0.01
S_7						1.00	0.31	-0.23
S_8							1.00	-0.13
S_9								1.00

Table 11: Correlation matrix for the CP -averaged observables from the maximum-likelihood fit in the bin $17.0 < q^2 < 19.0 \text{ GeV}^2/c^4$.

	F_L	S_3	S_4	S_5	A_{FB}	S_7	S_8	S_9
F_L	1.00	0.14	0.06	0.00	-0.35	0.02	-0.02	0.08
S_3		1.00	-0.04	-0.15	-0.12	-0.04	0.03	-0.04
S_4			1.00	0.25	-0.14	-0.10	0.08	0.02
S_5				1.00	-0.25	-0.07	-0.08	0.05
A_{FB}					1.00	-0.00	-0.03	-0.09
S_7						1.00	0.33	-0.09
S_8							1.00	-0.13
S_9								1.00

Table 12: Correlation matrix for the CP -averaged observables from the maximum-likelihood fit in the bin $1.1 < q^2 < 6.0 \text{ GeV}^2/c^4$.

	F_L	S_3	S_4	S_5	A_{FB}	S_7	S_8	S_9
F_L	1.00	-0.01	-0.02	0.00	0.01	-0.08	0.02	0.03
S_3		1.00	-0.04	-0.01	0.04	0.03	0.00	-0.02
S_4			1.00	-0.07	-0.09	0.01	0.01	-0.03
S_5				1.00	-0.07	0.00	0.01	-0.04
A_{FB}					1.00	-0.01	-0.03	-0.03
S_7						1.00	-0.02	-0.04
S_8							1.00	-0.08
S_9								1.00

Table 13: Correlation matrix for the CP -averaged observables from the maximum-likelihood fit in the bin $15.0 < q^2 < 19.0 \text{ GeV}^2/c^4$.

	F_L	S_3	S_4	S_5	A_{FB}	S_7	S_8	S_9
F_L	1.00	0.18	-0.06	-0.07	-0.37	0.00	-0.03	0.07
S_3		1.00	-0.04	-0.03	-0.07	-0.00	-0.04	0.02
S_4			1.00	0.21	-0.13	-0.03	0.04	0.06
S_5				1.00	-0.23	0.02	-0.01	0.04
A_{FB}					1.00	0.03	-0.01	0.00
S_7						1.00	0.28	-0.18
S_8							1.00	-0.14
S_9								1.00

4 Correlation matrices for the optimised angular observables

Correlation matrices between the optimised $P_i^{(r)}$ basis of observables in the different q^2 bins are provided in Tables 14–23.

Table 14: Correlation matrix for the optimised angular observables from the maximum-likelihood fit in the bin $0.10 < q^2 < 0.98 \text{ GeV}^2/c^4$.

	F_L	P_1	P_2	P_3	P'_4	P'_5	P'_6	P'_8
F_L	1.00	0.03	0.02	0.03	-0.08	-0.13	-0.02	0.06
P_1		1.00	0.02	0.01	0.02	0.14	-0.06	0.01
P_2			1.00	0.02	0.14	0.03	-0.02	-0.01
P_3				1.00	-0.01	-0.00	-0.10	-0.02
P'_4					1.00	0.07	-0.03	0.06
P'_5						1.00	-0.03	-0.02
P'_6							1.00	-0.04
P'_8								1.00

Table 15: Correlation matrix for the optimised angular observables from the maximum-likelihood fit in the bin $1.1 < q^2 < 2.5 \text{ GeV}^2/c^4$.

	F_L	P_1	P_2	P_3	P'_4	P'_5	P'_6	P'_8
F_L	1.00	-0.23	-0.51	0.26	0.03	0.24	-0.13	-0.13
P_1		1.00	0.15	-0.23	-0.00	-0.02	0.11	0.11
P_2			1.00	-0.09	-0.03	-0.22	0.05	0.14
P_3				1.00	0.07	0.19	-0.17	-0.00
P'_4					1.00	-0.20	0.02	-0.09
P'_5						1.00	-0.12	-0.04
P'_6							1.00	-0.14
P'_8								1.00

Table 16: Correlation matrix for the optimised angular observables from the maximum-likelihood fit in the bin $2.5 < q^2 < 4.0 \text{ GeV}^2/c^4$.

	F_L	P_1	P_2	P_3	P'_4	P'_5	P'_6	P'_8
F_L	1.00	0.08	-0.34	0.01	-0.21	-0.09	-0.08	-0.06
P_1		1.00	0.02	-0.02	-0.07	-0.03	0.00	-0.08
P_2			1.00	0.07	-0.02	-0.05	0.08	-0.03
P_3				1.00	0.02	-0.04	-0.04	0.07
P'_4					1.00	-0.10	0.02	0.04
P'_5						1.00	0.01	0.02
P'_6							1.00	0.01
P'_8								1.00

Table 17: Correlation matrix for the optimised angular observables from the maximum-likelihood fit in the bin $4.0 < q^2 < 6.0 \text{ GeV}^2/c^4$.

	F_L	P_1	P_2	P_3	P'_4	P'_5	P'_6	P'_8
F_L	1.00	0.04	0.05	-0.10	-0.04	-0.14	-0.17	0.14
P_1		1.00	0.06	0.07	-0.06	-0.10	-0.03	0.02
P_2			1.00	-0.02	-0.14	-0.09	-0.03	-0.01
P_3				1.00	-0.01	0.07	0.19	-0.01
P'_4					1.00	0.02	0.04	0.01
P'_5						1.00	0.09	0.00
P'_6							1.00	0.02
P'_8								1.00

Table 18: Correlation matrix for the optimised angular observables from the maximum-likelihood fit in the bin $6.0 < q^2 < 8.0 \text{ GeV}^2/c^4$.

	F_L	P_1	P_2	P_3	P'_4	P'_5	P'_6	P'_8
F_L	1.00	-0.02	0.17	0.01	-0.14	-0.18	-0.08	-0.02
P_1		1.00	0.01	0.10	-0.12	-0.23	0.04	0.04
P_2			1.00	-0.00	-0.13	-0.21	-0.06	0.02
P_3				1.00	0.03	0.06	0.09	0.08
P'_4					1.00	0.15	0.03	-0.03
P'_5						1.00	0.00	0.02
P'_6							1.00	0.08
P'_8								1.00

Table 19: Correlation matrix for the optimised angular observables from the maximum-likelihood fit in the bin $11.0 < q^2 < 12.5 \text{ GeV}^2/c^4$.

	F_L	P_1	P_2	P_3	P'_4	P'_5	P'_6	P'_8
F_L	1.00	-0.07	0.13	-0.07	0.04	-0.07	0.03	0.00
P_1		1.00	-0.09	0.10	0.07	-0.06	0.01	0.05
P_2			1.00	-0.16	-0.12	-0.23	-0.05	-0.11
P_3				1.00	0.01	0.18	0.10	0.00
P'_4					1.00	0.08	0.03	-0.02
P'_5						1.00	0.03	0.00
P'_6							1.00	0.27
P'_8								1.00

Table 20: Correlation matrix for the optimised angular observables from the maximum-likelihood fit in the bin $15.0 < q^2 < 17.0 \text{ GeV}^2/c^4$.

	F_L	P_1	P_2	P_3	P'_4	P'_5	P'_6	P'_8
F_L	1.00	0.06	0.14	-0.06	0.18	0.23	-0.01	-0.04
P_1		1.00	0.03	-0.09	-0.04	0.00	-0.03	-0.04
P_2			1.00	-0.06	-0.13	-0.25	0.01	-0.03
P_3				1.00	-0.04	-0.05	0.23	0.13
P'_4					1.00	0.32	0.02	0.06
P'_5						1.00	0.06	0.03
P'_6							1.00	0.31
P'_8								1.00

Table 21: Correlation matrix for the optimised angular observables from the maximum-likelihood fit in the bin $17.0 < q^2 < 19.0 \text{ GeV}^2/c^4$.

	F_L	P_1	P_2	P_3	P'_4	P'_5	P'_6	P'_8
F_L	1.00	-0.10	0.16	-0.01	0.22	0.14	-0.01	-0.01
P_1		1.00	-0.10	0.05	-0.07	-0.16	-0.05	0.03
P_2			1.00	0.06	-0.09	-0.23	0.00	-0.05
P_3				1.00	-0.01	-0.06	0.09	0.14
P'_4					1.00	0.27	-0.09	0.08
P'_5						1.00	-0.07	-0.09
P'_6							1.00	0.34
P'_8								1.00

Table 22: Correlation matrix for the optimised angular observables from the maximum-likelihood fit in the bin $1.1 < q^2 < 6.0 \text{ GeV}^2/c^4$.

	F_L	P_1	P_2	P_3	P'_4	P'_5	P'_6	P'_8
F_L	1.00	-0.05	-0.33	0.09	-0.11	-0.03	-0.14	0.02
P_1		1.00	0.05	0.02	-0.04	-0.00	0.03	0.01
P_2			1.00	-0.00	-0.04	-0.06	0.03	-0.04
P_3				1.00	0.02	0.03	0.03	0.08
P'_4					1.00	-0.06	0.03	0.01
P'_5						1.00	0.01	0.00
P'_6							1.00	-0.02
P'_8								1.00

Table 23: Correlation matrix for the optimised angular observables from the maximum-likelihood fit in the bin $15.0 < q^2 < 19.0 \text{ GeV}^2/c^4$.

	F_L	P_1	P_2	P_3	P'_4	P'_5	P'_6	P'_8
F_L	1.00	-0.08	0.19	-0.02	0.11	0.09	-0.01	-0.04
P_1		1.00	-0.01	-0.00	-0.04	-0.02	0.00	-0.04
P_2			1.00	-0.04	-0.14	-0.25	0.03	-0.03
P_3				1.00	-0.06	-0.04	0.18	0.14
P'_4					1.00	0.21	-0.03	0.04
P'_5						1.00	0.02	-0.01
P'_6							1.00	0.28
P'_8								1.00

5 Fit projections of the signal channel

The angular and mass distributions of the candidates in bins of q^2 for the Run 1 and the 2016 data, along with the projections of the simultaneous fit, are shown in Figs. 5–14.

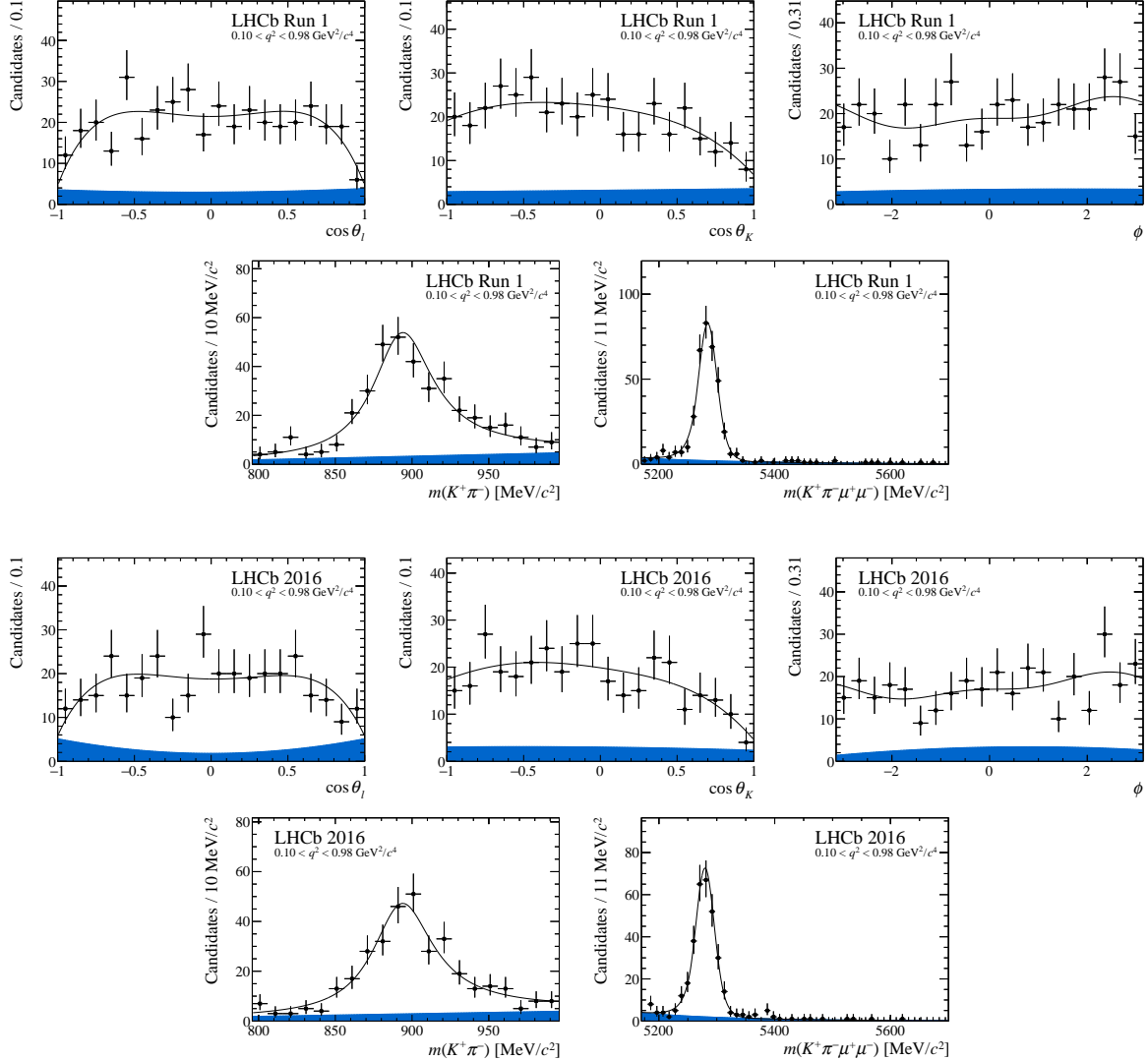


Figure 5: Projections of the fitted probability density function on the decay angles, $m(K^+\pi^-)$ and $m(K^+\pi^-\mu^+\mu^-)$ for the bin $0.10 < q^2 < 0.98 \text{ GeV}^2/c^4$. The blue shaded region indicates background.

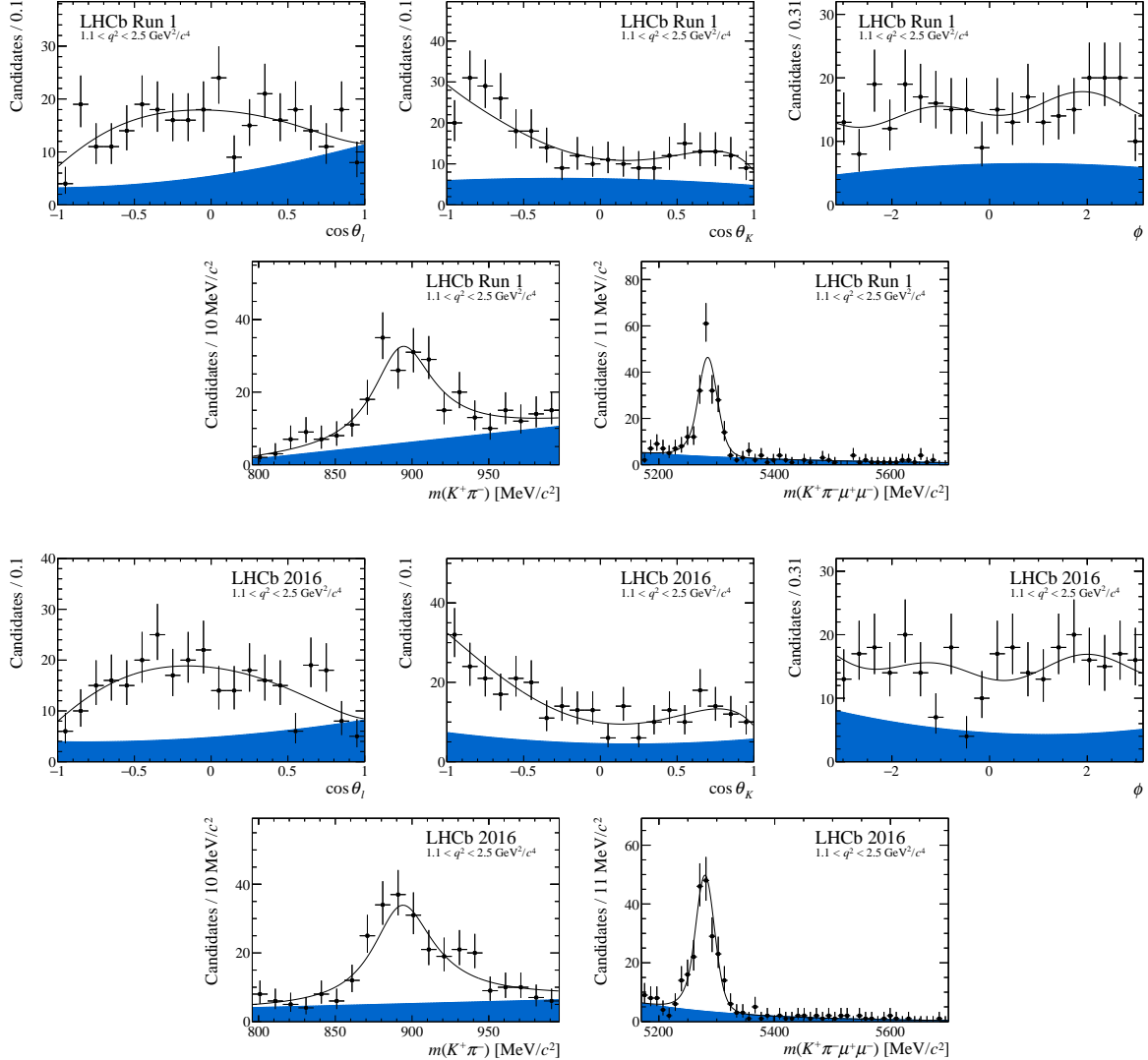


Figure 6: Projections of the fitted probability density function on the decay angles, $m(K^+\pi^-)$ and $m(K^+\pi^-\mu^+\mu^-)$ for the bin $1.1 < q^2 < 2.5 \text{ GeV}^2/c^4$. The blue shaded region indicates background.

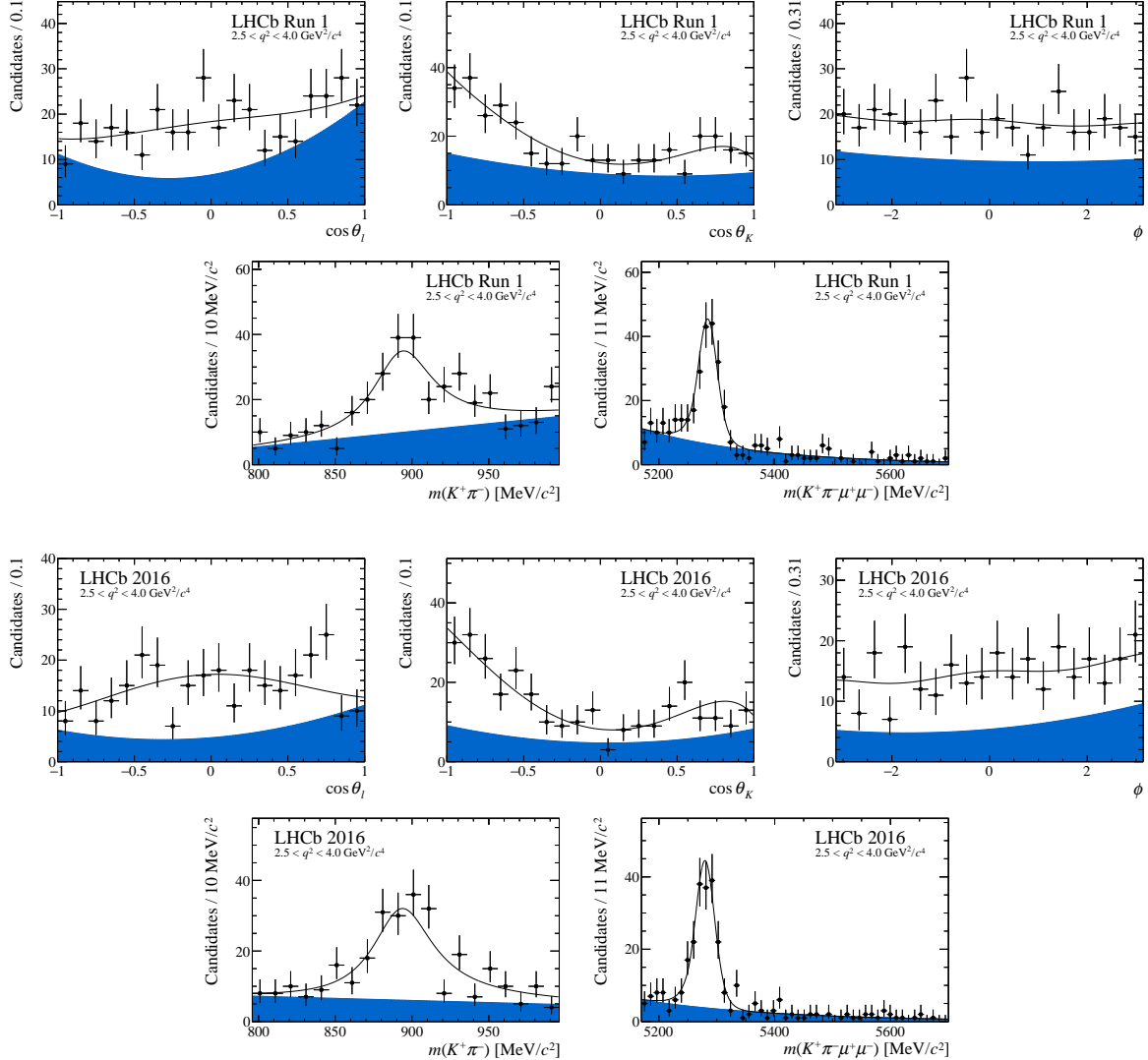


Figure 7: Projections of the fitted probability density function on the decay angles, $m(K^+\pi^-)$ and $m(K^+\pi^-\mu^+\mu^-)$ for the bin $2.5 < q^2 < 4.0 \text{ GeV}^2/c^4$. The blue shaded region indicates background.

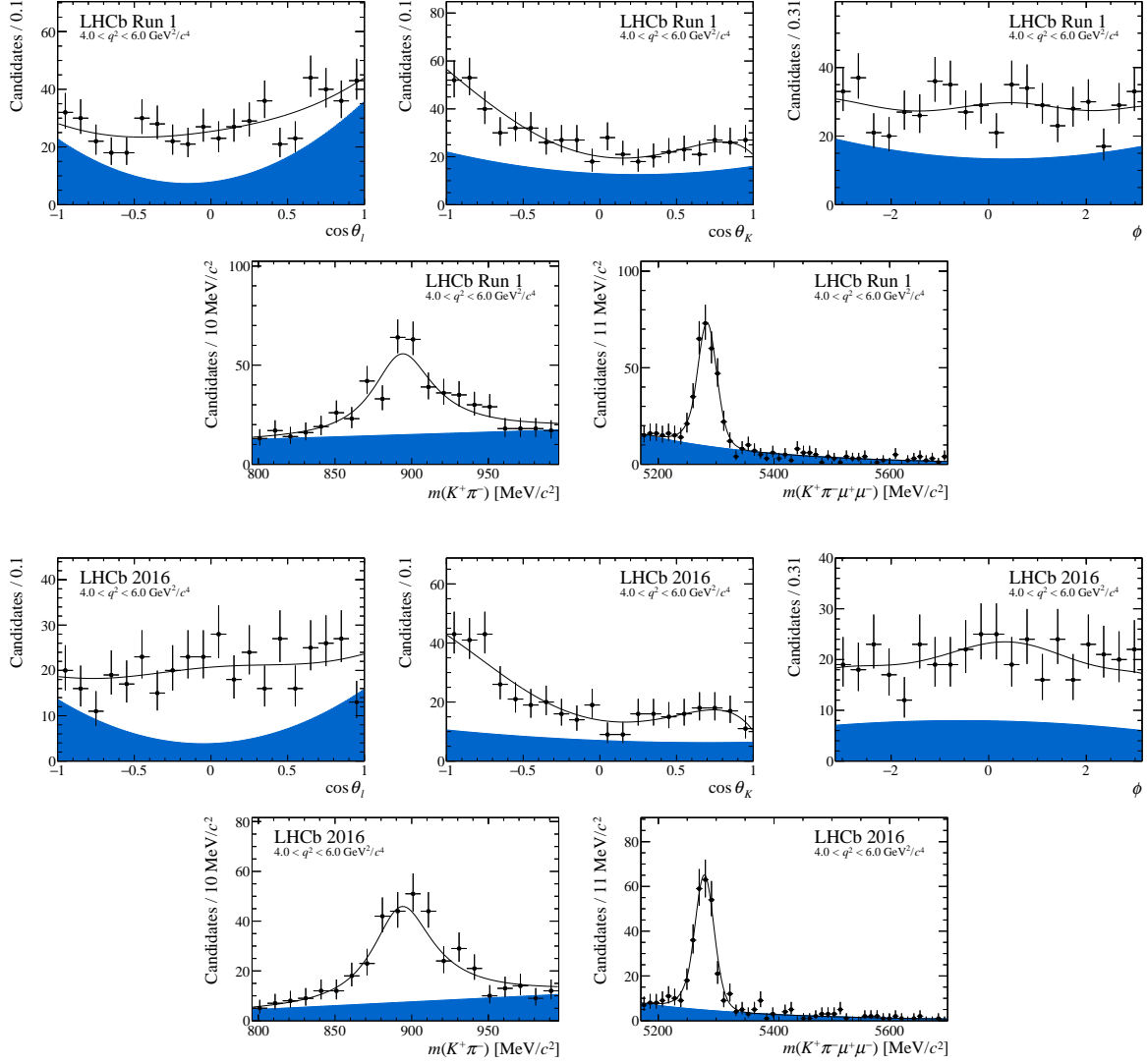


Figure 8: Projections of the fitted probability density function on the decay angles, $m(K^+\pi^-)$ and $m(K^+\pi^-\mu^+\mu^-)$ for the bin $4.0 < q^2 < 6.0 \text{ GeV}^2/c^4$. The blue shaded region indicates background.

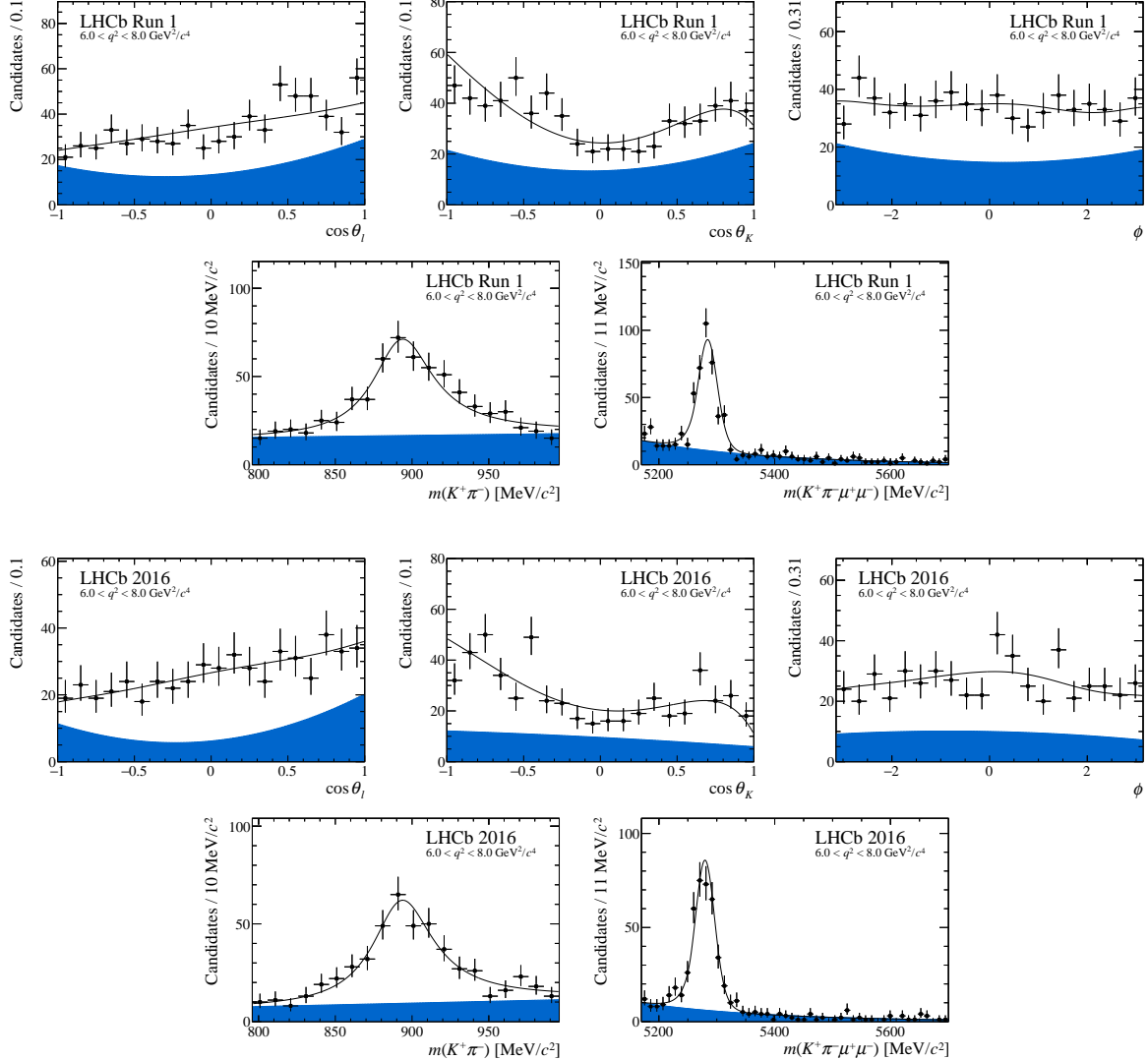


Figure 9: Projections of the fitted probability density function on the decay angles, $m(K^+\pi^-)$ and $m(K^+\pi^-\mu^+\mu^-)$ for the bin $6.0 < q^2 < 8.0 \text{ GeV}^2/c^4$. The blue shaded region indicates background.

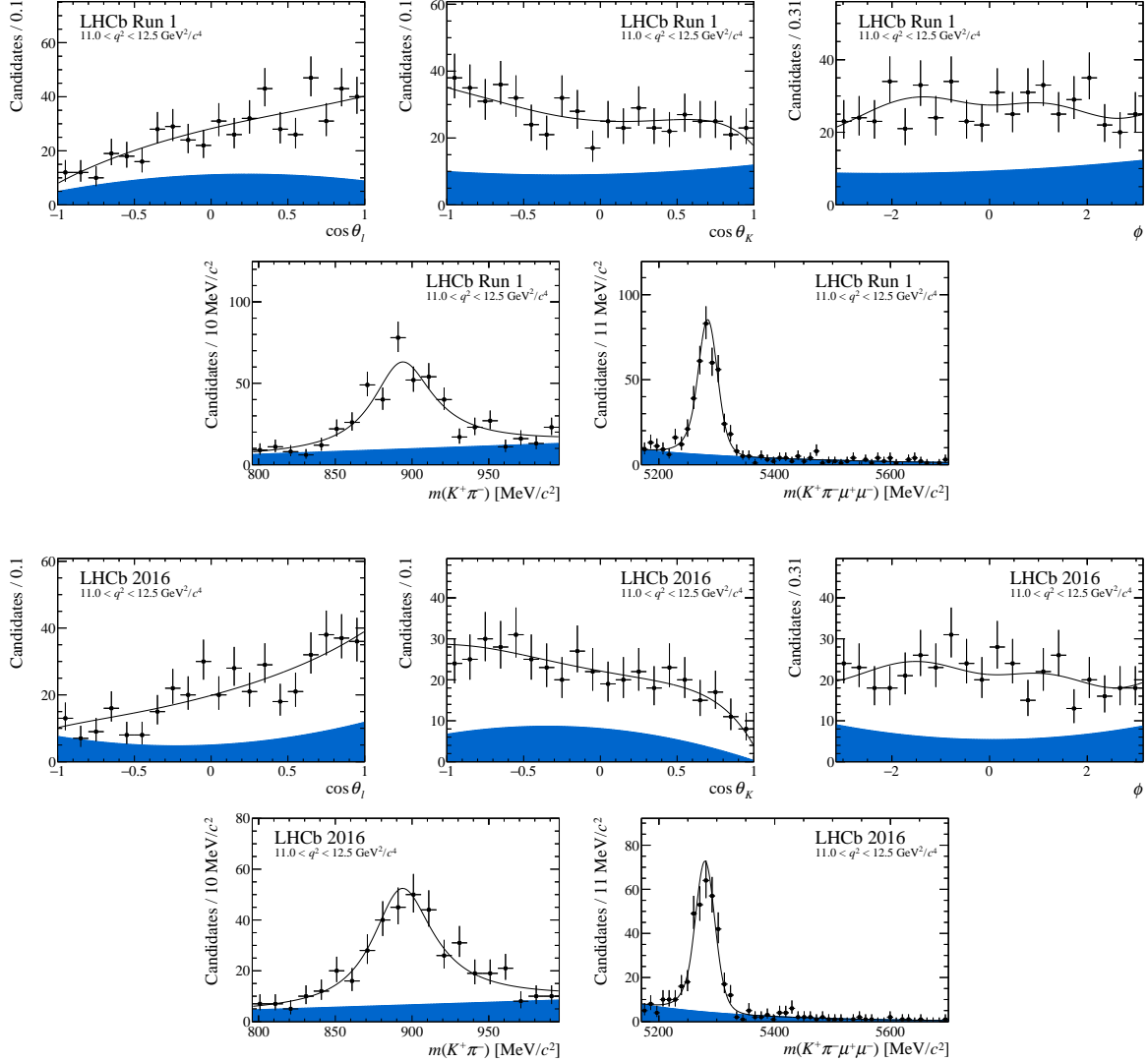


Figure 10: Projections of the fitted probability density function on the decay angles, $m(K^+\pi^-)$ and $m(K^+\pi^-\mu^+\mu^-)$ for the bin $11.0 < q^2 < 12.5 \text{ GeV}^2/c^4$. The blue shaded region indicates background.

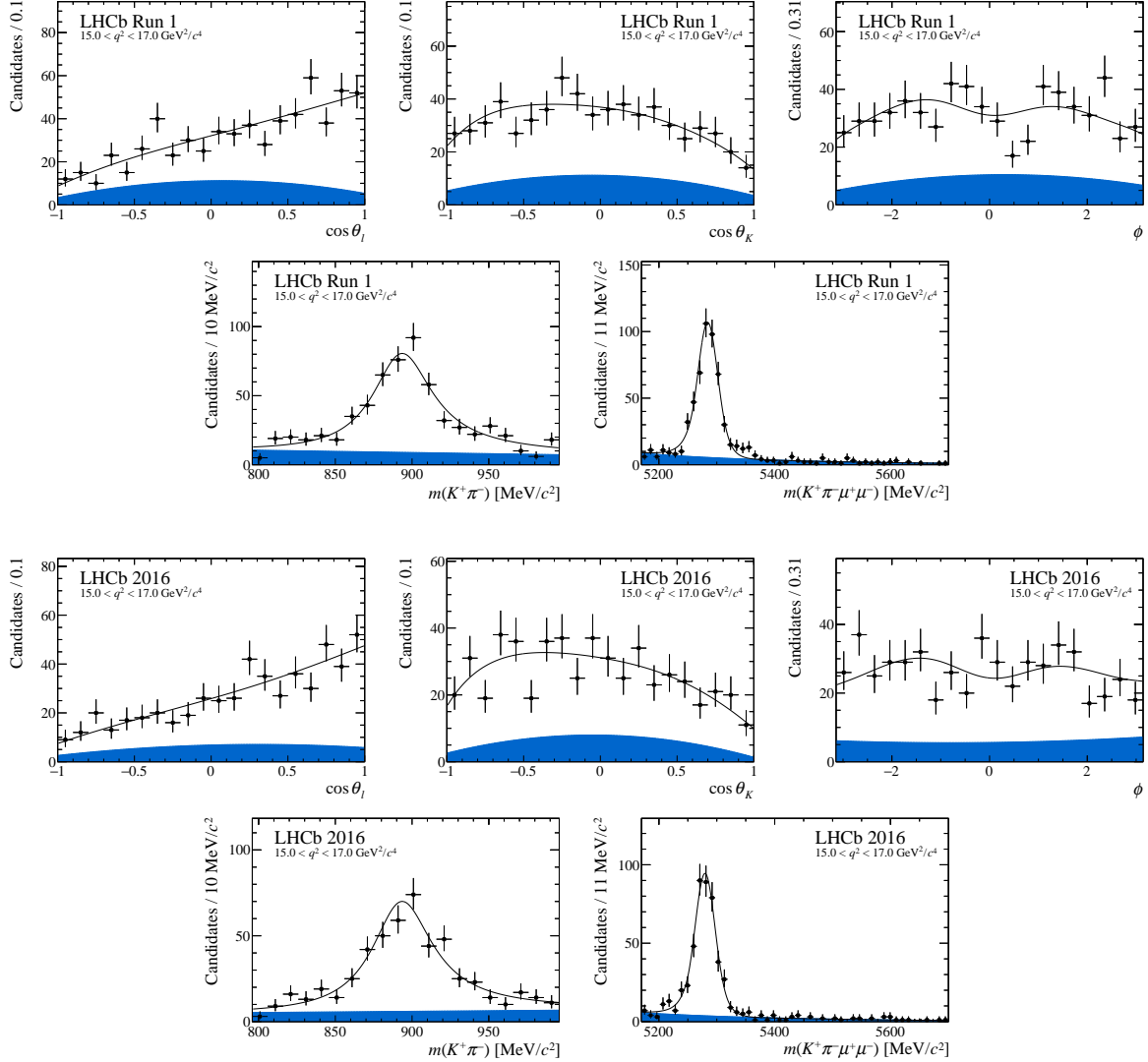


Figure 11: Projections of the fitted probability density function on the decay angles, $m(K^+\pi^-)$ and $m(K^+\pi^-\mu^+\mu^-)$ for the bin $15.0 < q^2 < 17.0 \text{ GeV}^2/c^4$. The blue shaded region indicates background.

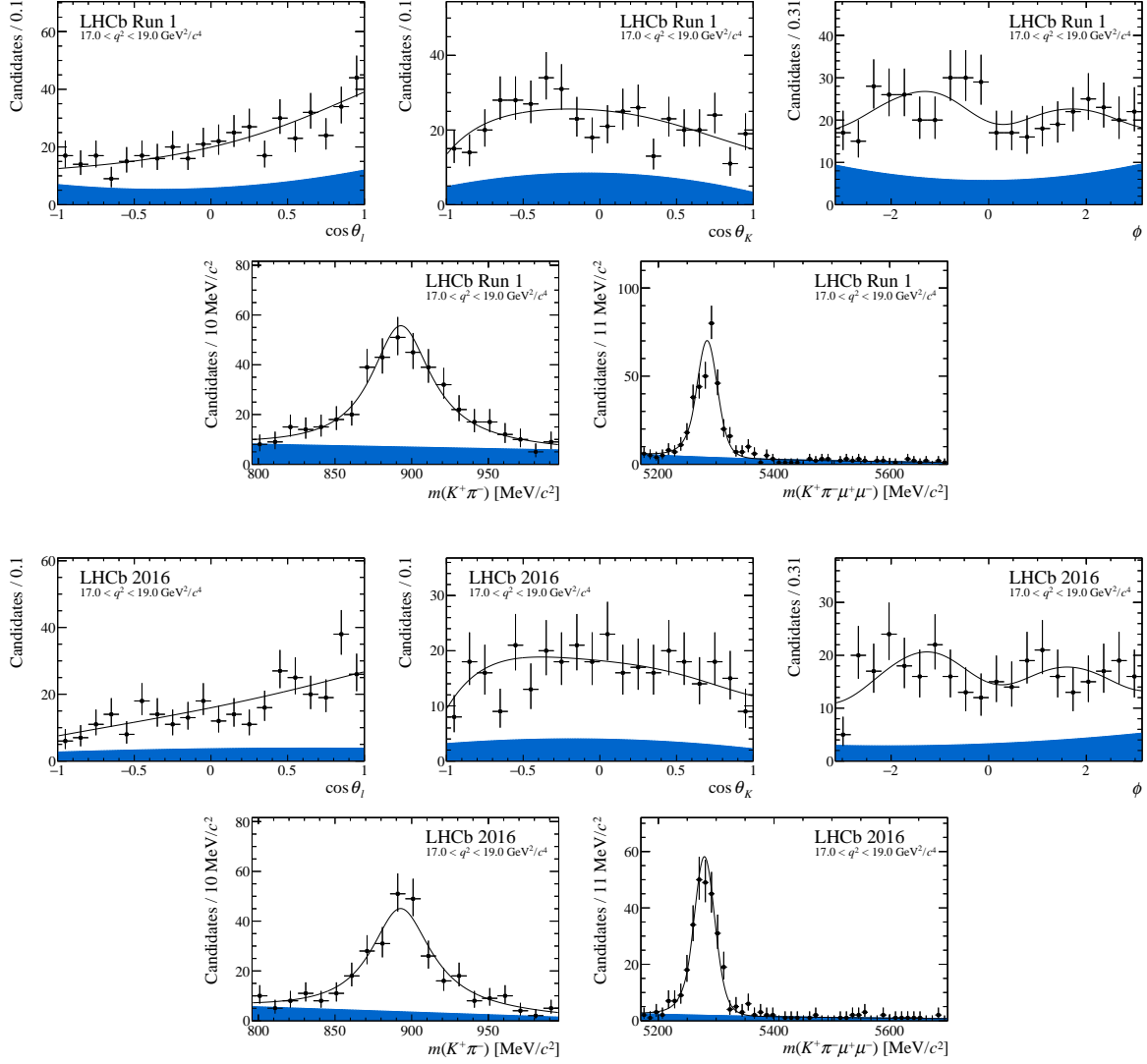


Figure 12: Projections of the fitted probability density function on the decay angles, $m(K^+\pi^-)$ and $m(K^+\pi^-\mu^+\mu^-)$ for the bin $17.0 < q^2 < 19.0 \text{ GeV}^2/c^4$. The blue shaded region indicates background.

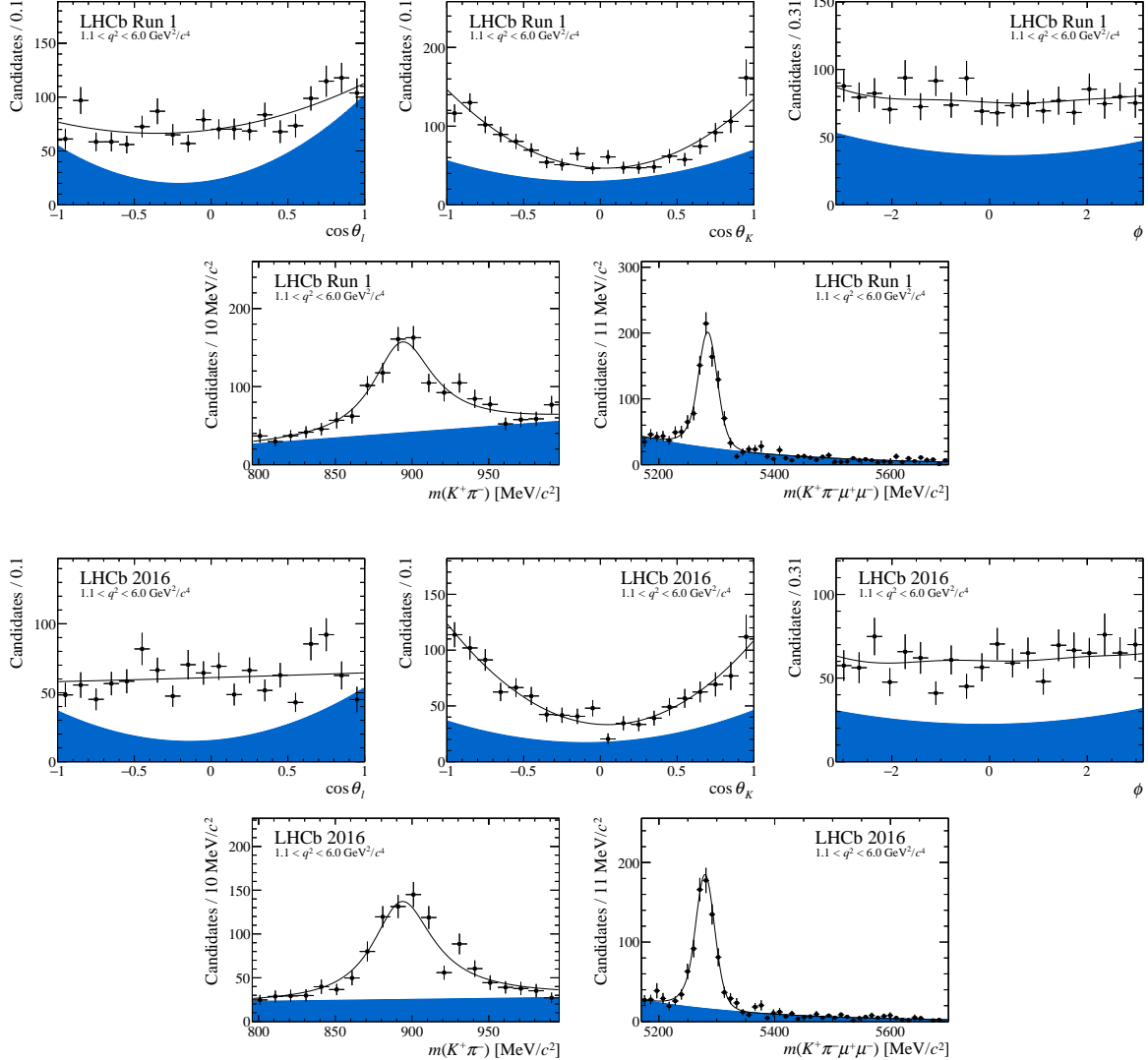


Figure 13: Projections of the fitted probability density function on the decay angles, $m(K^+\pi^-)$ and $m(K^+\pi^-\mu^+\mu^-)$ for the bin $1.1 < q^2 < 6.0 \text{ GeV}^2/c^4$. The blue shaded region indicates background.

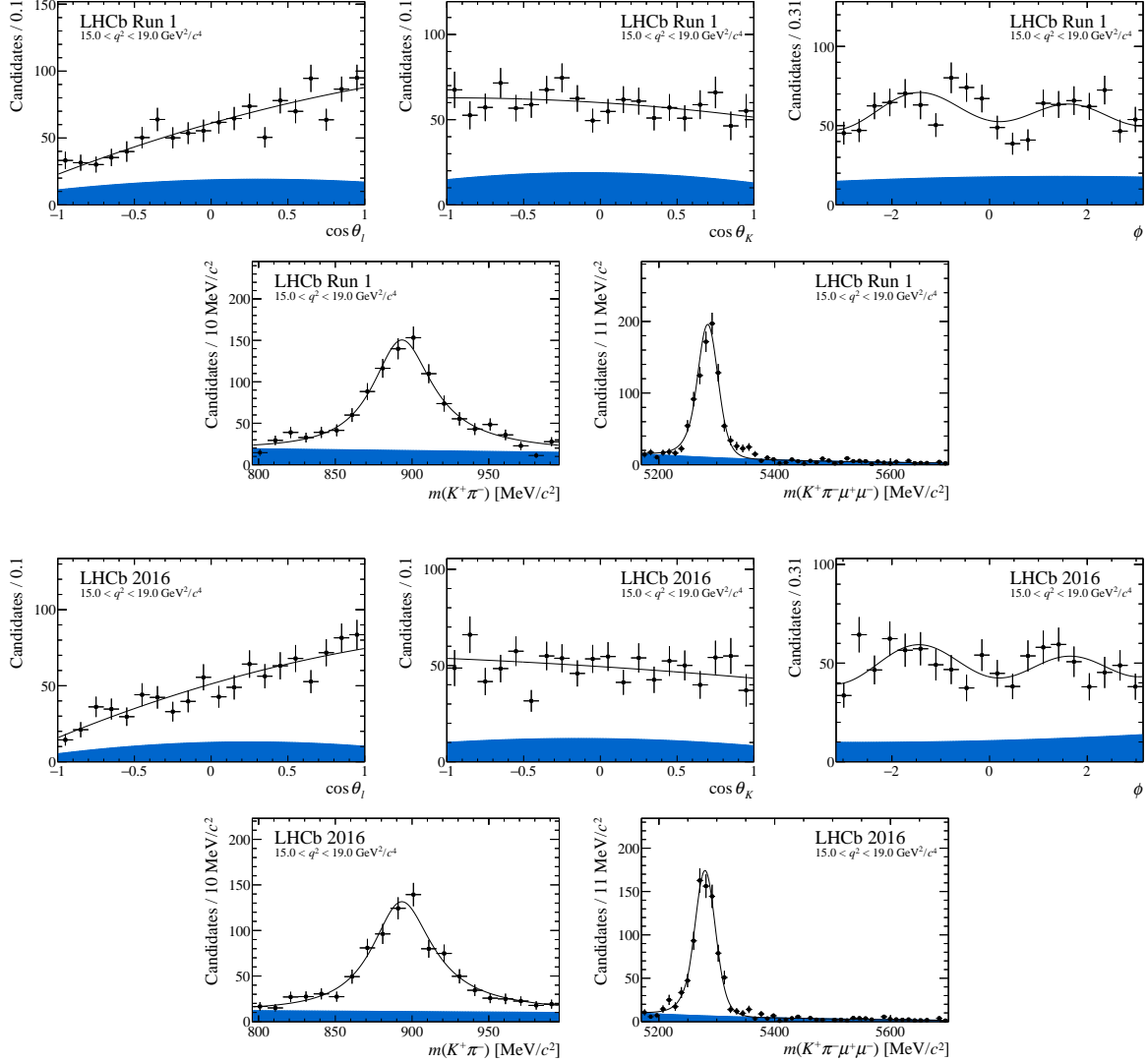


Figure 14: Projections of the fitted probability density function on the decay angles, $m(K^+\pi^-)$ and $m(K^+\pi^-\mu^+\mu^-)$ for the bin $15.0 < q^2 < 19.0 \text{ GeV}^2/c^4$. The blue shaded region indicates background.

References

- [1] LHCb collaboration, R. Aaij *et al.*, *Angular analysis of the $B^0 \rightarrow K^{*0} \mu^+ \mu^-$ decay using 3 fb^{-1} of integrated luminosity*, JHEP **02** (2016) 104, [arXiv:1512.04442](#).
- [2] CMS collaboration, A. M. Sirunyan *et al.*, *Measurement of angular parameters from the decay $B^0 \rightarrow K^{*0} \mu^+ \mu^-$ in proton-proton collisions at $\sqrt{s} = 8 \text{ TeV}$* , Phys. Lett. **B781** (2018) 517, [arXiv:1710.02846](#).
- [3] ATLAS collaboration, M. Aaboud *et al.*, *Angular analysis of $B_d^0 \rightarrow K^* \mu^+ \mu^-$ decays in pp collisions at $\sqrt{s} = 8 \text{ TeV}$ with the ATLAS detector*, JHEP **10** (2018) 047, [arXiv:1805.04000](#).
- [4] Belle collaboration, S. Wehle *et al.*, *Lepton-flavor-dependent angular analysis of $B \rightarrow K^* \ell^+ \ell^-$* , Phys. Rev. Lett. **118** (2017) 111801, [arXiv:1612.05014](#).
- [5] BaBar collaboration, B. Aubert *et al.*, *Measurements of branching fractions, rate asymmetries, and angular distributions in the rare decays $B \rightarrow K \ell^+ \ell^-$ and $B \rightarrow K^* \ell^+ \ell^-$* , Phys. Rev. **D73** (2006) 092001, [arXiv:hep-ex/0604007](#).
- [6] CDF collaboration, T. Aaltonen *et al.*, *Measurements of the angular distributions in the decays $B \rightarrow K^{(*)} \mu^+ \mu^-$ at CDF*, Phys. Rev. Lett. **108** (2012) 081807, [arXiv:1108.0695](#).
- [7] LHCb collaboration, R. Aaij *et al.*, *Angular moments of the decay $\Lambda_b^0 \rightarrow \Lambda \mu^+ \mu^-$ at low hadronic recoil*, JHEP **09** (2018) 146, [arXiv:1808.00264](#).
- [8] LHCb collaboration, R. Aaij *et al.*, *Angular analysis and differential branching fraction of the decay $B_s^0 \rightarrow \phi \mu^+ \mu^-$* , JHEP **09** (2015) 179, [arXiv:1506.08777](#).
- [9] LHCb collaboration, R. Aaij *et al.*, *Measurements of the S-wave fraction in $B^0 \rightarrow K^+ \pi^- \mu^+ \mu^-$ decays and the $B^0 \rightarrow K^*(892)^0 \mu^+ \mu^-$ differential branching fraction*, JHEP **11** (2016) 047, Erratum *ibid.* **04** (2017) 142, [arXiv:1606.04731](#).
- [10] LHCb collaboration, R. Aaij *et al.*, *Differential branching fraction and angular analysis of $\Lambda_b^0 \rightarrow \Lambda \mu^+ \mu^-$ decays*, JHEP **06** (2015) 115, Erratum *ibid.* **09** (2018) 145, [arXiv:1503.07138](#).
- [11] LHCb collaboration, R. Aaij *et al.*, *Differential branching fractions and isospin asymmetries of $B \rightarrow K^{(*)} \mu^+ \mu^-$ decays*, JHEP **06** (2014) 133, [arXiv:1403.8044](#).
- [12] LHCb collaboration, R. Aaij *et al.*, *Search for lepton-universality violation in $B^+ \rightarrow K^+ \ell^+ \ell^-$ decays*, Phys. Rev. Lett. **122** (2019) 191801, [arXiv:1903.09252](#).
- [13] Belle collaboration, A. Abdesselam *et al.*, *Test of lepton flavor universality in $B \rightarrow K \ell^+ \ell^-$ decays*, [arXiv:1908.01848](#).
- [14] BaBar collaboration, J. P. Lees *et al.*, *Measurement of branching fractions and rate asymmetries in the rare decays $B \rightarrow K^{(*)} \ell^+ \ell^-$* , Phys. Rev. **D86** (2012) 032012, [arXiv:1204.3933](#).

- [15] LHCb collaboration, R. Aaij *et al.*, *Test of lepton universality with $B^0 \rightarrow K^{*0} \ell^+ \ell^-$ decays*, JHEP **08** (2017) 055, [arXiv:1705.05802](#).
- [16] Belle collaboration, A. Abdesselam *et al.*, *Test of lepton flavor universality in $B \rightarrow K^* \ell^+ \ell^-$ decays at Belle*, [arXiv:1904.02440](#).
- [17] M. Algueró *et al.*, *Emerging patterns of new physics with and without Lepton flavour universal contributions*, Eur. Phys. J. **C79** (2019) 714, [arXiv:1903.09578](#).
- [18] J. Aebischer *et al.*, *B -decay discrepancies after Moriond 2019*, [arXiv:1903.10434](#).
- [19] A. Arbey *et al.*, *Update on the $b \rightarrow s$ anomalies*, Phys. Rev. **D100** (2019) 015045, [arXiv:1904.08399](#).
- [20] M. Ciuchini *et al.*, *New physics in $b \rightarrow s \ell^+ \ell^-$ confronts new data on lepton universality*, Eur. Phys. J. **C79** (2019) 719, [arXiv:1903.09632](#).
- [21] K. Kowalska, D. Kumar, and E. M. Sessolo, *Implications for new physics in $b \rightarrow s \mu \mu$ transitions after recent measurements by Belle and LHCb*, Eur. Phys. J. **C79** (2019) 840, [arXiv:1903.10932](#).
- [22] A. K. Alok, A. Dighe, S. Gangal, and D. Kumar, *Continuing search for new physics in $b \rightarrow s \mu \mu$ decays: Two operators at a time*, JHEP **06** (2019) 089, [arXiv:1903.09617](#).
- [23] W. Altmannshofer, S. Gori, M. Pospelov, and I. Yavin, *Quark flavor transitions in $L_\mu - L_\tau$ models*, Phys. Rev. **D89** (2014) 095033, [arXiv:1403.1269](#).
- [24] A. Crivellin, G. D'Ambrosio, and J. Heeck, *Explaining $h \rightarrow \mu^\pm \tau^\mp$, $B \rightarrow K^* \mu^+ \mu^-$ and $B \rightarrow K \mu^+ \mu^- / B \rightarrow K e^+ e^-$ in a two-Higgs-doublet model with gauged $L_\mu - L_\tau$* , Phys. Rev. Lett. **114** (2015) 151801, [arXiv:1501.00993](#).
- [25] A. Celis, J. Fuentes-Martín, M. Jung, and H. Serôdio, *Family nonuniversal Z' models with protected flavor-changing interactions*, Phys. Rev. **D92** (2015) 015007, [arXiv:1505.03079](#).
- [26] A. Falkowski, M. Nardecchia, and R. Ziegler, *Lepton flavor non-universality in B -meson decays from a $U(2)$ flavor model*, JHEP **11** (2015) 173, [arXiv:1509.01249](#).
- [27] G. Hiller and M. Schmaltz, *R_K and future $b \rightarrow s \ell \ell$ physics beyond the standard model opportunities*, Phys. Rev. **D90** (2014) 054014, [arXiv:1408.1627](#).
- [28] B. Gripaios, M. Nardecchia, and S. A. Renner, *Composite leptoquarks and anomalies in B -meson decays*, JHEP **05** (2015) 006, [arXiv:1412.1791](#).
- [29] I. de Medeiros Varzielas and G. Hiller, *Clues for flavor from rare lepton and quark decays*, JHEP **06** (2015) 072, [arXiv:1503.01084](#).
- [30] R. Barbieri, C. W. Murphy, and F. Senia, *B -decay anomalies in a composite leptoquark model*, Eur. Phys. J. **C77** (2017) 8, [arXiv:1611.04930](#).
- [31] J.-H. Sheng, R.-M. Wang, and Y.-D. Yang, *Scalar leptoquark effects in the lepton flavor violating exclusive $b \rightarrow s \ell_i^- \ell_j^+$ Decays*, Int. J. Theor. Phys. **58** (2019) 480, [arXiv:1805.05059](#).

- [32] G. Hiller, D. Loose, and I. Nišandžić, *Flavorful leptoquarks at hadron colliders*, Phys. Rev. **D97** (2018) 075004, [arXiv:1801.09399](#).
- [33] A. Crivellin, D. Müller, and T. Ota, *Simultaneous explanation of $R(D^{(*)})$ and $b \rightarrow s\mu^+\mu^-$: the last scalar leptoquarks standing*, JHEP **09** (2017) 040, [arXiv:1703.09226](#).
- [34] F. Sala and D. M. Straub, *A new light particle in B decays?*, Phys. Lett. **B774** (2017) 205209.
- [35] P. Ko, Y. Omura, Y. Shigekami, and C. Yu, *LHCb anomaly and B physics in flavored Z' models with flavored Higgs doublets*, Phys. Rev. **D95** (2017) 115040.
- [36] S. Jäger and J. Martin Camalich, *Reassessing the discovery potential of the $B \rightarrow K^*\ell^+\ell^-$ decays in the large-recoil region: SM challenges and BSM opportunities*, Phys. Rev. **D93** (2016) 014028, [arXiv:1412.3183](#).
- [37] J. Lyon and R. Zwicky, *Resonances gone topsy turvy - the charm of QCD or new physics in $b \rightarrow s\ell^+\ell^-$?*, [arXiv:1406.0566](#).
- [38] M. Ciuchini *et al.*, *$B \rightarrow K^*\ell^+\ell^-$ decays at large recoil in the Standard Model: a theoretical reappraisal*, JHEP **06** (2016) 116, [arXiv:1512.07157](#).
- [39] C. Bobeth, M. Chrzaszcz, D. van Dyk, and J. Virto, *Long-distance effects in $B \rightarrow K^*\ell\ell$ from analyticity*, Eur. Phys. J. **C78** (2018) 451, [arXiv:1707.07305](#).
- [40] F. Beaujean, C. Bobeth, and D. van Dyk, *Comprehensive Bayesian analysis of rare (semi)leptonic and radiative B decays*, Eur. Phys. J. **C74** (2014) 2897, [arXiv:1310.2478](#).
- [41] C. Bobeth, G. Hiller, and D. van Dyk, *The benefits of $\bar{B} \rightarrow \bar{K}^*l^+l^-$ decays at low recoil*, JHEP **07** (2010) 098, [arXiv:1006.5013](#).
- [42] D. M. Straub, *flavio: A python package for flavour and precision phenomenology in the Standard Model and beyond*, [arXiv:1810.08132](#).
- [43] A. Bharucha, D. M. Straub, and R. Zwicky, *$B \rightarrow V\ell^+\ell^-$ in the Standard Model from light-cone sum rules*, JHEP **08** (2016) 098, [arXiv:1503.05534](#).
- [44] W. Altmannshofer and D. M. Straub, *New physics in $b \rightarrow s$ transitions after LHC run 1*, Eur. Phys. J. **C75** (2015) 382, [arXiv:1411.3161](#).
- [45] LHCb collaboration, R. Aaij *et al.*, *Differential branching fraction and angular analysis of the decay $B^0 \rightarrow K^{*0}\mu^+\mu^-$* , JHEP **08** (2013) 131, [arXiv:1304.6325](#).
- [46] W. Altmannshofer *et al.*, *Symmetries and asymmetries of $B \rightarrow K^*\mu^+\mu^-$ decays in the Standard Model and beyond*, JHEP **01** (2009) 019, [arXiv:0811.1214](#).
- [47] S. Descotes-Genon, J. Matias, M. Ramon, and J. Virto, *Implications from clean observables for the binned analysis of $B \rightarrow K^*\mu^+\mu^-$ at large recoil*, JHEP **01** (2013) 048, [arXiv:1207.2753](#).

- [48] LHCb collaboration, A. A. Alves Jr. *et al.*, *The LHCb detector at the LHC*, JINST **3** (2008) S08005.
- [49] LHCb collaboration, R. Aaij *et al.*, *LHCb detector performance*, Int. J. Mod. Phys. **A30** (2015) 1530022, [arXiv:1412.6352](#).
- [50] T. Sjöstrand, S. Mrenna, and P. Skands, *PYTHIA 6.4 physics and manual*, JHEP **05** (2006) 026, [arXiv:hep-ph/0603175](#); T. Sjöstrand, S. Mrenna, and P. Skands, *A brief introduction to PYTHIA 8.1*, Comput. Phys. Commun. **178** (2008) 852, [arXiv:0710.3820](#).
- [51] I. Belyaev *et al.*, *Handling of the generation of primary events in Gauss, the LHCb simulation framework*, J. Phys. Conf. Ser. **331** (2011) 032047.
- [52] D. J. Lange, *The EvtGen particle decay simulation package*, Nucl. Instrum. Meth. **A462** (2001) 152.
- [53] P. Golonka and Z. Was, *PHOTOS Monte Carlo: A precision tool for QED corrections in Z and W decays*, Eur. Phys. J. **C45** (2006) 97, [arXiv:hep-ph/0506026](#).
- [54] Geant4 collaboration, J. Allison *et al.*, *Geant4 developments and applications*, IEEE Trans. Nucl. Sci. **53** (2006) 270; Geant4 collaboration, S. Agostinelli *et al.*, *Geant4: A simulation toolkit*, Nucl. Instrum. Meth. **A506** (2003) 250.
- [55] M. Clemencic *et al.*, *The LHCb simulation application, Gauss: Design, evolution and experience*, J. Phys. Conf. Ser. **331** (2011) 032023.
- [56] L. Anderlini *et al.*, *The PIDCalib package*, LHCb-PUB-2016-021, CERN, Geneva, 2016.
- [57] R. Aaij *et al.*, *Selection and processing of calibration samples to measure the particle identification performance of the LHCb experiment in Run 2*, EPJ Tech. Instrum. **6** (2019) 1, [arXiv:1803.00824](#).
- [58] R. Aaij *et al.*, *The LHCb trigger and its performance in 2011*, JINST **8** (2013) P04022, [arXiv:1211.3055](#).
- [59] L. Breiman, J. H. Friedman, R. A. Olshen, and C. J. Stone, *Classification and regression trees*, Wadsworth international group, Belmont, California, USA, 1984.
- [60] Y. Freund and R. E. Schapire, *A decision-theoretic generalization of on-line learning and an application to boosting*, J. Comput. Syst. Sci. **55** (1997) 119.
- [61] A. Blum, A. Kalai, and J. Langford, *Beating the hold-out: Bounds for k-fold and progressive cross-validation*, in *Proceedings of the Twelfth Annual Conference on Computational Learning Theory*, COLT '99, (New York, NY, USA), 203–208, ACM, 1999.
- [62] LHCb collaboration, R. Aaij *et al.*, *Search for the rare decays $B_s^0 \rightarrow \mu^+ \mu^-$ and $B^0 \rightarrow \mu^+ \mu^-$* , Phys. Lett. **B699** (2011) 330, [arXiv:1103.2465](#).
- [63] B. Efron, *Bootstrap methods: Another look at the jackknife*, Ann. Statist. **7** (1979) 1.

- [64] LHCb collaboration, R. Aaij *et al.*, *Evidence for the decay $B_s^0 \rightarrow \bar{K}^{*0}\mu^+\mu^-$* , JHEP **07** (2018) 020, [arXiv:1804.07167](#).
- [65] D. Aston *et al.*, *A Study of $K^-\pi^+$ scattering in the reaction $K^-\pi^+ \rightarrow K^-\pi^+n$ at 11 GeV/c*, Nucl. Phys. **B296** (1988) 493.
- [66] BaBar collaboration, B. Aubert *et al.*, *Measurement of decay amplitudes of $B \rightarrow J/\psi K^*, \psi(2S)K^*$, and $\chi_{c1}K^*$ with an angular analysis*, Phys. Rev. **D76** (2007) 031102, [arXiv:0704.0522](#).
- [67] Belle collaboration, K. Chilikin *et al.*, *Observation of a new charged charmonium like state in $\bar{B}^0 \rightarrow J/\psi K^-\pi^+$ decays*, Phys. Rev. **D90** (2014) 112009, [arXiv:1408.6457](#).
- [68] LHCb collaboration, R. Aaij *et al.*, *Measurement of the polarization amplitudes in $B^0 \rightarrow J/\psi K^*(892)^0$ decays*, Phys. Rev. **D88** (2013) 052002, [arXiv:1307.2782](#).
- [69] S. Descotes-Genon, L. Hofer, J. Matias, and J. Virto, *On the impact of power corrections in the prediction of $B \rightarrow K^*\mu^+\mu^-$ observables*, JHEP **12** (2014) 125, [arXiv:1407.8526](#).
- [70] A. Khodjamirian, T. Mannel, A. A. Pivovarov, and Y.-M. Wang, *Charm-loop effect in $B \rightarrow K^{(*)}\ell^+\ell^-$ and $B \rightarrow K^*\gamma$* , JHEP **09** (2010) 089, [arXiv:1006.4945](#).
- [71] R. R. Horgan, Z. Liu, S. Meinel, and M. Wingate, *Lattice QCD calculation of form factors describing the rare decays $B \rightarrow K^*\ell^+\ell^-$ and $B_s \rightarrow \phi\ell^+\ell^-$* , Phys. Rev. **D89** (2014) 094501, [arXiv:1310.3722](#).
- [72] R. R. Horgan, Z. Liu, S. Meinel, and M. Wingate, *Rare B decays using lattice QCD form factors*, PoS LATTICE2014 (2015) 372, [arXiv:1501.00367](#).

LHCb collaboration

R. Aaij³¹, C. Abellán Beteta⁴⁹, T. Ackernley⁵⁹, B. Adeva⁴⁵, M. Adinolfi⁵³, H. Afsharnia⁹, C.A. Aidala⁸¹, S. Aiola²⁵, Z. Ajaltouni⁹, S. Akar⁶⁶, P. Albicocco²², J. Albrecht¹⁴, F. Alessio⁴⁷, M. Alexander⁵⁸, A. Alfonso Albero⁴⁴, G. Alkhazov³⁷, P. Alvarez Cartelle⁶⁰, A.A. Alves Jr⁴⁵, S. Amato², Y. Amhis¹¹, L. An²¹, L. Anderlini²¹, G. Andreassi⁴⁸, M. Andreotti²⁰, F. Archilli¹⁶, A. Artamonov⁴³, M. Artuso⁶⁷, K. Arzymatov⁴¹, E. Aslanides¹⁰, M. Atzeni⁴⁹, B. Audurier¹¹, S. Bachmann¹⁶, J.J. Back⁵⁵, S. Baker⁶⁰, V. Balagura^{11,b}, W. Baldini²⁰, A. Baranov⁴¹, R.J. Barlow⁶¹, S. Barsuk¹¹, W. Barter⁶⁰, M. Bartolini^{23,47,h}, F. Baryshnikov⁷⁸, J.M. Basels¹³, G. Bassi²⁸, V. Batozskaya³⁵, B. Batsukh⁶⁷, A. Battig¹⁴, A. Bay⁴⁸, M. Becker¹⁴, F. Bedeschi²⁸, I. Bediaga¹, A. Beiter⁶⁷, V. Belavin⁴¹, S. Belin²⁶, V. Bellee⁴⁸, K. Belous⁴³, I. Belyaev³⁸, G. Bencivenni²², E. Ben-Haim¹², S. Benson³¹, A. Berezhnoy³⁹, R. Bernet⁴⁹, D. Berninghoff¹⁶, H.C. Bernstein⁶⁷, C. Bertella⁴⁷, E. Bertholet¹², A. Bertolin²⁷, C. Betancourt⁴⁹, F. Betti^{19,e}, M.O. Bettler⁵⁴, Ia. Bezshyiko⁴⁹, S. Bhasin⁵³, J. Bhom³³, M.S. Bieker¹⁴, S. Bifani⁵², P. Billoir¹², A. Bizzeti^{21,t}, M. Bjørn⁶², M.P. Blago⁴⁷, T. Blake⁵⁵, F. Blanc⁴⁸, S. Blusk⁶⁷, D. Bobulska⁵⁸, V. Bocci³⁰, O. Boente Garcia⁴⁵, T. Boettcher⁶³, A. Boldyrev⁷⁹, A. Bondar^{42,w}, N. Bondar^{37,47}, S. Borghi⁶¹, M. Borisjak⁴¹, M. Borsato¹⁶, J.T. Borsuk³³, T.J.V. Bowcock⁵⁹, C. Bozzi²⁰, M.J. Bradley⁶⁰, S. Braun⁶⁵, A. Brea Rodriguez⁴⁵, M. Brodski⁴⁷, J. Brodzicka³³, A. Brossa Gonzalo⁵⁵, D. Brundu²⁶, E. Buchanan⁵³, A. Büchler-Germann⁴⁹, A. Buonaura⁴⁹, C. Burr⁴⁷, A. Bursche²⁶, A. Butkevich⁴⁰, J.S. Butter³¹, J. Buytaert⁴⁷, W. Byczynski⁴⁷, S. Cadeddu²⁶, H. Cai⁷², R. Calabrese^{20,g}, L. Calero Diaz²², S. Cali²², R. Calladine⁵², M. Calvi^{24,i}, M. Calvo Gomez^{44,l}, P. Camargo Magalhaes⁵³, A. Camboni^{44,l}, P. Campana²², D.H. Campora Perez³¹, A.F. Campoverde Quezada⁵, L. Capriotti^{19,e}, A. Carbone^{19,e}, G. Carboni²⁹, R. Cardinale^{23,h}, A. Cardini²⁶, I. Carli⁶, P. Carniti^{24,i}, K. Carvalho Akiba³¹, A. Casais Vidal⁴⁵, G. Casse⁵⁹, M. Cattaneo⁴⁷, G. Cavallero⁴⁷, S. Celani⁴⁸, R. Cenci^{28,o}, J. Cerasoli¹⁰, M.G. Chapman⁵³, M. Charles¹², Ph. Charpentier⁴⁷, G. Chatzikonstantinidis⁵², M. Chefdeville⁸, V. Chekalina⁴¹, C. Chen³, S. Chen²⁶, A. Chernov³³, S.-G. Chitic⁴⁷, V. Chobanova⁴⁵, S. Cholak⁴⁸, M. Chrzaszcz³³, A. Chubykin³⁷, V. Chulikov³⁷, P. Ciambrone²², M.F. Cicala⁵⁵, X. Cid Vidal⁴⁵, G. Ciezarek⁴⁷, F. Cindolo¹⁹, P.E.L. Clarke⁵⁷, M. Clemencic⁴⁷, H.V. Cliff⁵⁴, J. Closier⁴⁷, J.L. Cobbley⁶¹, V. Coco⁴⁷, J.A.B. Coelho¹¹, J. Cogan¹⁰, E. Cogneras⁹, L. Cojocariu³⁶, P. Collins⁴⁷, T. Colombo⁴⁷, A. Contu²⁶, N. Cooke⁵², G. Coombs⁵⁸, S. Coquereau⁴⁴, G. Corti⁴⁷, C.M. Costa Sobral⁵⁵, B. Couturier⁴⁷, D.C. Craik⁶³, J. Crkovská⁶⁶, A. Crocombe⁵⁵, M. Cruz Torres^{1,z}, R. Currie⁵⁷, C.L. Da Silva⁶⁶, E. Dall'Occo¹⁴, J. Dalseno^{45,53}, C. D'Ambrosio⁴⁷, A. Danilina³⁸, P. d'Argent⁴⁷, A. Davis⁶¹, O. De Aguiar Francisco⁴⁷, K. De Bruyn⁴⁷, S. De Capua⁶¹, M. De Cian⁴⁸, J.M. De Miranda¹, L. De Paula², M. De Serio^{18,d}, P. De Simone²², J.A. de Vries⁷⁶, C.T. Dean⁶⁶, W. Dean⁸¹, D. Decamp⁸, L. Del Buono¹², B. Delaney⁵⁴, H.-P. Dembinski¹⁴, A. Dendek³⁴, V. Denysenko⁴⁹, D. Derkach⁷⁹, O. Deschamps⁹, F. Desse¹¹, F. Dettori^{26,f}, B. Dey⁷, A. Di Canto⁴⁷, P. Di Nezza²², S. Didenko⁷⁸, H. Dijkstra⁴⁷, V. Dobishuk⁵¹, F. Dordei²⁶, M. Dorigo^{28,x}, A.C. dos Reis¹, L. Douglas⁵⁸, A. Dovbnya⁵⁰, K. Dreimanis⁵⁹, M.W. Dudek³³, L. Dufour⁴⁷, P. Durante⁴⁷, J.M. Durham⁶⁶, D. Dutta⁶¹, M. Dziewiecki¹⁶, A. Dziurda³³, A. Dzyuba³⁷, S. Easo⁵⁶, U. Egede⁶⁹, V. Egorychev³⁸, S. Eidelman^{42,w}, S. Eisenhardt⁵⁷, S. Ek-In⁴⁸, L. Eklund⁵⁸, S. Ely⁶⁷, A. Ene³⁶, E. Epple⁶⁶, S. Escher¹³, J. Eschle⁴⁹, S. Esen³¹, T. Evans⁴⁷, A. Falabella¹⁹, J. Fan³, Y. Fan⁵, N. Farley⁵², S. Farry⁵⁹, D. Fazzini¹¹, P. Fedin³⁸, M. Féo⁴⁷, P. Fernandez Declara⁴⁷, A. Fernandez Prieto⁴⁵, F. Ferrari^{19,e}, L. Ferreira Lopes⁴⁸, F. Ferreira Rodrigues², S. Ferreres Sole³¹, M. Ferrillo⁴⁹, M. Ferro-Luzzi⁴⁷, S. Filippov⁴⁰, R.A. Fini¹⁸, M. Fiorini^{20,g}, M. Firlej³⁴, K.M. Fischer⁶², C. Fitzpatrick⁴⁷, T. Fiutowski³⁴, F. Fleuret^{11,b}, M. Fontana⁴⁷, F. Fontanelli^{23,h}, R. Forty⁴⁷, V. Franco Lima⁵⁹, M. Franco Sevilla⁶⁵, M. Frank⁴⁷, C. Frei⁴⁷, D.A. Friday⁵⁸, J. Fu^{25,p}, Q. Fuehring¹⁴, W. Funk⁴⁷, E. Gabriel⁵⁷, T. Gaintseva⁴¹, A. Gallas Torreira⁴⁵, D. Galli^{19,e}, S. Gallorini²⁷, S. Gambetta⁵⁷, Y. Gan³, M. Gandelman²,

P. Gandini²⁵, Y. Gao⁴, L.M. Garcia Martin⁴⁶, J. García Pardiñas⁴⁹, B. Garcia Plana⁴⁵,
 F.A. Garcia Rosales¹¹, L. Garrido⁴⁴, D. Gascon⁴⁴, C. Gaspar⁴⁷, D. Gerick¹⁶, E. Gersabeck⁶¹,
 M. Gersabeck⁶¹, T. Gershon⁵⁵, D. Gerstel¹⁰, Ph. Ghez⁸, V. Gibson⁵⁴, A. Gioventù⁴⁵,
 P. Gironella Gironell⁴⁴, L. Giubega³⁶, C. Giugliano²⁰, K. Gizdov⁵⁷, V.V. Gligorov¹², C. Göbel⁷⁰,
 D. Golubkov³⁸, A. Golutvin^{60,78}, A. Gomes^{1,a}, P. Gorbounov³⁸, I.V. Gorelov³⁹, C. Gotti^{24,i},
 E. Govorkova³¹, J.P. Grabowski¹⁶, R. Graciani Diaz⁴⁴, T. Grammatico¹²,
 L.A. Granado Cardoso⁴⁷, E. Graugés⁴⁴, E. Graverini⁴⁸, G. Graziani²¹, A. Grecu³⁶, R. Greim³¹,
 P. Griffith²⁰, L. Grillo⁶¹, L. Gruber⁴⁷, B.R. Gruberg Cazon⁶², C. Gu³, E. Gushchin⁴⁰,
 A. Guth¹³, Yu. Guz^{43,47}, T. Gys⁴⁷, P. A. Gnther¹⁶, T. Hadavizadeh⁶², G. Haefeli⁴⁸, C. Haen⁴⁷,
 S.C. Haines⁵⁴, P.M. Hamilton⁶⁵, Q. Han⁷, X. Han¹⁶, T.H. Hancock⁶², S. Hansmann-Menzemer¹⁶,
 N. Harnew⁶², T. Harrison⁵⁹, R. Hart³¹, C. Hasse¹⁴, M. Hatch⁴⁷, J. He⁵, M. Hecker⁶⁰,
 K. Heijhoff³¹, K. Heinicke¹⁴, A.M. Hennequin⁴⁷, K. Hennessy⁵⁹, L. Henry^{25,46}, J. Heuel¹³,
 A. Hicheur⁶⁸, D. Hill⁶², M. Hilton⁶¹, P.H. Hopchev⁴⁸, J. Hu¹⁶, J. Hu⁷¹, W. Hu⁷, W. Huang⁵,
 W. Hulsbergen³¹, T. Humair⁶⁰, R.J. Hunter⁵⁵, M. Hushchyn⁷⁹, D. Hutchcroft⁵⁹, D. Hynds³¹,
 P. Ibis¹⁴, M. Idzik³⁴, P. Ilten⁵², A. Inglessi³⁷, K. Ivshin³⁷, R. Jacobsson⁴⁷, S. Jakobsen⁴⁷,
 E. Jans³¹, B.K. Jashai⁴⁶, A. Jawahery⁶⁵, V. Jevtic¹⁴, F. Jiang³, M. John⁶², D. Johnson⁴⁷,
 C.R. Jones⁵⁴, B. Jost⁴⁷, N. Jurik⁶², S. Kandybei⁵⁰, M. Karacson⁴⁷, J.M. Kariuki⁵³, N. Kazeev⁷⁹,
 M. Kecke¹⁶, F. Keizer^{54,47}, M. Kelsey⁶⁷, M. Kenzie⁵⁵, T. Ketel³², B. Khanji⁴⁷, A. Kharisova⁸⁰,
 K.E. Kim⁶⁷, T. Kirn¹³, V.S. Kirsebom⁴⁸, S. Klaver²², K. Klimaszewski³⁵, S. Koliiev⁵¹,
 A. Kondybayeva⁷⁸, A. Konoplyannikov³⁸, P. Kopciewicz³⁴, R. Kopecna¹⁶, P. Koppenburg³¹,
 M. Korolev³⁹, I. Kostiuk^{31,51}, O. Kot⁵¹, S. Kotriakhova³⁷, L. Kravchuk⁴⁰, R.D. Krawczyk⁴⁷,
 M. Kreps⁵⁵, F. Kress⁶⁰, S. Kretzschmar¹³, P. Krokovny^{42,w}, W. Krupa³⁴, W. Krzemien³⁵,
 W. Kucewicz^{33,k}, M. Kucharczyk³³, V. Kudryavtsev^{42,w}, H.S. Kuindersma³¹, G.J. Kunde⁶⁶,
 T. Kvaratskheliya³⁸, D. Lacarrere⁴⁷, G. Lafferty⁶¹, A. Lai²⁶, D. Lancierini⁴⁹, J.J. Lane⁶¹,
 G. Lanfranchi²², C. Langenbruch¹³, O. Lantwin⁴⁹, T. Latham⁵⁵, F. Lazzari^{28,u}, R. Le Gac¹⁰,
 S.H. Lee⁸¹, R. Lefèvre⁹, A. Leflat^{39,47}, O. Leroy¹⁰, T. Lesiak³³, B. Leverington¹⁶, H. Li⁷¹,
 L. Li⁶², X. Li⁶⁶, Y. Li⁶, Z. Li⁶⁷, X. Liang⁶⁷, T. Lin⁶⁰, R. Lindner⁴⁷, V. Lisovskyi¹⁴, G. Liu⁷¹,
 X. Liu³, D. Loh⁵⁵, A. Loi²⁶, J. Lomba Castro⁴⁵, I. Longstaff⁵⁸, J.H. Lopes², G. Loustau⁴⁹,
 G.H. Lovell⁵⁴, Y. Lu⁶, D. Lucchesi^{27,n}, M. Lucio Martinez³¹, Y. Luo³, A. Lupato²⁷, E. Luppi^{20,g},
 O. Lupton⁵⁵, A. Lusiani^{28,s}, X. Lyu⁵, S. Maccolini^{19,e}, F. Machefert¹¹, F. Maciuc³⁶, V. Macko⁴⁸,
 P. Mackowiak¹⁴, S. Maddrell-Mander⁵³, L.R. Madhan Mohan⁵³, O. Maev³⁷, A. Maevskiy⁷⁹,
 D. Maisuzenko³⁷, M.W. Majewski³⁴, S. Malde⁶², B. Malecki⁴⁷, A. Malinin⁷⁷, T. Maltsev^{42,w},
 H. Malygina¹⁶, G. Manca^{26,f}, G. Mancinelli¹⁰, R. Manera Escalero⁴⁴, D. Manuzzi^{19,e},
 D. Marangotto²⁵, J. Maratas^{9,v}, J.F. Marchand⁸, U. Marconi¹⁹, S. Mariani^{21,21,47},
 C. Marin Benito¹¹, M. Marinangeli⁴⁸, P. Marino⁴⁸, J. Marks¹⁶, P.J. Marshall⁵⁹, G. Martellotti³⁰,
 L. Martinazzoli⁴⁷, M. Martinelli^{24,i}, D. Martinez Santos⁴⁵, F. Martinez Vidal⁴⁶, A. Massafferri¹,
 M. Materok¹³, R. Matev⁴⁷, A. Mathad⁴⁹, Z. Mathe⁴⁷, V. Matiunin³⁸, C. Matteuzzi²⁴,
 K.R. Mattioli⁸¹, A. Mauri⁴⁹, E. Maurice^{11,b}, M. McCann⁶⁰, L. Mcconnell¹⁷, A. McNab⁶¹,
 R. McNulty¹⁷, J.V. Mead⁵⁹, B. Meadows⁶⁴, C. Meaux¹⁰, G. Meier¹⁴, N. Meinert⁷⁴,
 D. Melnychuk³⁵, S. Meloni^{24,i}, M. Merk³¹, A. Merli²⁵, M. Mikhasenko⁴⁷, D.A. Milanes⁷³,
 E. Millard⁵⁵, M.-N. Minard⁸, O. Mineev³⁸, L. Minzoni²⁰, S.E. Mitchell⁵⁷, B. Mitreska⁶¹,
 D.S. Mitzel⁴⁷, A. Mödden¹⁴, A. Mogini¹², R.D. Moise⁶⁰, T. Mombächer¹⁴, I.A. Monroy⁷³,
 S. Monteil⁹, M. Morandin²⁷, G. Morello²², M.J. Morello^{28,s}, J. Moron³⁴, A.B. Morris¹⁰,
 A.G. Morris⁵⁵, R. Mountain⁶⁷, H. Mu³, F. Muheim⁵⁷, M. Mukherjee⁷, M. Mulder⁴⁷,
 D. Müller⁴⁷, K. Müller⁴⁹, C.H. Murphy⁶², D. Murray⁶¹, P. Muzzetto²⁶, P. Naik⁵³, T. Nakada⁴⁸,
 R. Nandakumar⁵⁶, T. Nanut⁴⁸, I. Nasteva², M. Needham⁵⁷, N. Neri^{25,p}, S. Neubert¹⁶,
 N. Neufeld⁴⁷, R. Newcombe⁶⁰, T.D. Nguyen⁴⁸, C. Nguyen-Mau^{48,m}, E.M. Niel¹¹, S. Nieswand¹³,
 N. Nikitin³⁹, N.S. Nolte⁴⁷, C. Nunez⁸¹, A. Oblakowska-Mucha³⁴, V. Obraztsov⁴³, S. Ogilvy⁵⁸,
 D.P. O'Hanlon⁵³, R. Oldeman^{26,f}, C.J.G. Onderwater⁷⁵, J. D. Osborn⁸¹, A. Ossowska³³,
 J.M. Otalora Goicochea², T. Ovsiannikova³⁸, P. Owen⁴⁹, A. Oyanguren⁴⁶, P.R. Pais⁴⁸,

T. Pajero^{28,28,47,s}, A. Palano¹⁸, M. Palutan²², G. Panshin⁸⁰, A. Papanestis⁵⁶, M. Pappagallo⁵⁷,
 L.L. Pappalardo²⁰, C. Pappenheimer⁶⁴, W. Parker⁶⁵, C. Parkes⁶¹, G. Passaleva^{21,47},
 A. Pastore¹⁸, M. Patel⁶⁰, C. Patrignani^{19,e}, A. Pearce⁴⁷, A. Pellegrino³¹, M. Pepe Altarelli⁴⁷,
 S. Perazzini¹⁹, D. Pereima³⁸, P. Perret⁹, L. Pescatore⁴⁸, K. Petridis⁵³, A. Petrolini^{23,h},
 A. Petrov⁷⁷, S. Petrucci⁵⁷, M. Petruzzo^{25,p}, B. Pietrzyk⁸, G. Pietrzyk⁴⁸, M. Pili⁶², D. Pinci³⁰,
 J. Pinzino⁴⁷, F. Pisani¹⁹, A. Piucci¹⁶, V. Placinta³⁶, S. Playfer⁵⁷, J. Plews⁵², M. Plo Casasus⁴⁵,
 F. Polci¹², M. Poli Lener²², M. Poliakova⁶⁷, A. Poluektov¹⁰, N. Polukhina^{78,c}, I. Polyakov⁶⁷,
 E. Polycarpo², G.J. Pomery⁵³, S. Ponce⁴⁷, A. Popov⁴³, D. Popov⁵², S. Poslavskii⁴³,
 K. Prasant³³, L. Promberger⁴⁷, C. Prouve⁴⁵, V. Pugatch⁵¹, A. Puig Navarro⁴⁹, H. Pullen⁶²,
 G. Punzi^{28,o}, W. Qian⁵, J. Qin⁵, R. Quagliani¹², B. Quintana⁸, N.V. Raab¹⁷,
 R.I. Rabadan Trejo¹⁰, B. Rachwal³⁴, J.H. Rademacker⁵³, M. Rama²⁸, M. Ramos Pernas⁴⁵,
 M.S. Rangel², F. Ratnikov^{41,79}, G. Raven³², M. Reboud⁸, F. Redi⁴⁸, F. Reiss¹²,
 C. Remon Alepuz⁴⁶, Z. Ren³, V. Renaudin⁶², S. Ricciardi⁵⁶, D.S. Richards⁵⁶, S. Richards⁵³,
 K. Rinnert⁵⁹, P. Robbe¹¹, A. Robert¹², A.B. Rodrigues⁴⁸, E. Rodrigues⁵⁹,
 J.A. Rodriguez Lopez⁷³, M. Roehrken⁴⁷, A. Rollings⁶², V. Romanovskiy⁴³, M. Romero Lamas⁴⁵,
 A. Romero Vidal⁴⁵, J.D. Roth⁸¹, M. Rotondo²², M.S. Rudolph⁶⁷, T. Ruf⁴⁷, J. Ruiz Vidal⁴⁶,
 A. Ryzhikov⁷⁹, J. Ryzka³⁴, J.J. Saborido Silva⁴⁵, N. Sagidova³⁷, N. Sahoo⁵⁵, B. Saitta^{26,f},
 C. Sanchez Gras³¹, C. Sanchez Mayordomo⁴⁶, R. Santacesaria³⁰, C. Santamarina Rios⁴⁵,
 M. Santimaria²², E. Santovetti^{29,j}, G. Sarpis⁶¹, M. Sarpis¹⁶, A. Sarti³⁰, C. Satriano^{30,r},
 A. Satta²⁹, M. Saur⁵, D. Savrina^{38,39}, L.G. Scantlebury Smead⁶², S. Schael¹³, M. Schellenberg¹⁴,
 M. Schiller⁵⁸, H. Schindler⁴⁷, M. Schmelling¹⁵, T. Schmelzer¹⁴, B. Schmidt⁴⁷, O. Schneider⁴⁸,
 A. Schopper⁴⁷, H.F. Schreiner⁶⁴, M. Schubiger³¹, S. Schulte⁴⁸, M.H. Schune¹¹, R. Schwemmer⁴⁷,
 B. Sciascia²², A. Sciubba²², S. Sellam⁶⁸, A. Semennikov³⁸, A. Sergi^{52,47}, N. Serra⁴⁹,
 J. Serrano¹⁰, L. Sestini²⁷, A. Seuthe¹⁴, P. Seyfert⁴⁷, D.M. Shangase⁸¹, M. Shapkin⁴³,
 L. Shchutska⁴⁸, T. Shears⁵⁹, L. Shekhtman^{42,w}, V. Shevchenko⁷⁷, E. Shmanin⁷⁸,
 J.D. Shupperd⁶⁷, B.G. Siddi²⁰, R. Silva Coutinho⁴⁹, L. Silva de Oliveira², G. Simi^{27,n},
 S. Simone^{18,d}, I. Skiba²⁰, N. Skidmore¹⁶, T. Skwarnicki⁶⁷, M.W. Slater⁵², J.G. Smeaton⁵⁴,
 A. Smetkina³⁸, E. Smith¹³, I.T. Smith⁵⁷, M. Smith⁶⁰, A. Snoch³¹, M. Soares¹⁹,
 L. Soares Lavra⁹, M.D. Sokoloff⁶⁴, F.J.P. Soler⁵⁸, B. Souza De Paula², B. Spaan¹⁴,
 E. Spadaro Norella^{25,p}, P. Spradlin⁵⁸, F. Stagni⁴⁷, M. Stahl⁶⁴, S. Stahl⁴⁷, P. Steffko⁴⁸,
 O. Steinkamp^{49,78}, S. Stemmle¹⁶, O. Stenyakin⁴³, M. Stepanova³⁷, H. Stevens¹⁴, S. Stone⁶⁷,
 S. Stracka²⁸, M.E. Stramaglia⁴⁸, M. Straticiuc³⁶, S. Strokov⁸⁰, J. Sun²⁶, L. Sun⁷², Y. Sun⁶⁵,
 P. Svihra⁶¹, K. Swientek³⁴, A. Szabelski³⁵, T. Szumlak³⁴, M. Szymanski⁴⁷, S. Taneja⁶¹,
 Z. Tang³, T. Tekampe¹⁴, F. Teubert⁴⁷, E. Thomas⁴⁷, K.A. Thomson⁵⁹, M.J. Tilley⁶⁰,
 V. Tisserand⁹, S. T'Jampens⁸, M. Tobin⁶, S. Tolk⁴⁷, L. Tomassetti^{20,g}, D. Torres Machado¹,
 D.Y. Tou¹², E. Tournefier⁸, M. Traill⁵⁸, M.T. Tran⁴⁸, E. Trifonova⁷⁸, C. Tripl⁴⁸,
 A. Tsaregorodtsev¹⁰, G. Tuci^{28,o}, A. Tully⁴⁸, N. Tuning³¹, A. Ukleja³⁵, A. Usachov³¹,
 A. Ustyuzhanin^{41,79}, U. Uwer¹⁶, A. Vagner⁸⁰, V. Vagnoni¹⁹, A. Valassi⁴⁷, G. Valenti¹⁹,
 M. van Beuzekom³¹, H. Van Hecke⁶⁶, E. van Herwijnen⁴⁷, C.B. Van Hulse¹⁷, M. van Veghel⁷⁵,
 R. Vazquez Gomez⁴⁴, P. Vazquez Regueiro⁴⁵, C. Vázquez Sierra³¹, S. Vecchi²⁰, J.J. Velthuis⁵³,
 M. Veltri^{21,q}, A. Venkateswaran⁶⁷, M. Veronesi³¹, M. Vesterinen⁵⁵, J.V. Viana Barbosa⁴⁷,
 D. Vieira⁶⁴, M. Vieites Diaz⁴⁸, H. Viemann⁷⁴, X. Vilasis-Cardona^{44,l}, G. Vitali²⁸,
 A. Vitkovskiy³¹, A. Vollhardt⁴⁹, D. Vom Bruch¹², A. Vorobyev³⁷, V. Vorobyev^{42,w},
 N. Voropaev³⁷, R. Waldi⁷⁴, J. Walsh²⁸, J. Wang³, J. Wang⁷², J. Wang⁶, M. Wang³, Y. Wang⁷,
 Z. Wang⁴⁹, D.R. Ward⁵⁴, H.M. Wark⁵⁹, N.K. Watson⁵², D. Websdale⁶⁰, A. Weiden⁴⁹,
 C. Weisser⁶³, B.D.C. Westhenry⁵³, D.J. White⁶¹, M. Whitehead¹³, D. Wiedner¹⁴,
 G. Wilkinson⁶², M. Wilkinson⁶⁷, I. Williams⁵⁴, M. Williams⁶³, M.R.J. Williams⁶¹,
 T. Williams⁵², F.F. Wilson⁵⁶, W. Wislicki³⁵, M. Witek³³, L. Witola¹⁶, G. Wormser¹¹,
 S.A. Wotton⁵⁴, H. Wu⁶⁷, K. Wyllie⁴⁷, Z. Xiang⁵, D. Xiao⁷, Y. Xie⁷, H. Xing⁷¹, A. Xu⁴, J. Xu⁵,
 L. Xu³, M. Xu⁷, Q. Xu⁵, Z. Xu⁴, Z. Yang³, Z. Yang⁶⁵, Y. Yao⁶⁷, L.E. Yeomans⁵⁹, H. Yin⁷,

J. Yu⁷, X. Yuan⁶⁷, O. Yushchenko⁴³, K.A. Zarebski⁵², M. Zavertyaev^{15,c}, M. Zdybal³³, M. Zeng³, D. Zhang⁷, L. Zhang³, S. Zhang⁴, W.C. Zhang^{3,y}, Y. Zhang⁴⁷, A. Zhelezov¹⁶, Y. Zheng⁵, X. Zhou⁵, Y. Zhou⁵, X. Zhu³, V. Zhukov^{13,39}, J.B. Zonneveld⁵⁷, S. Zucchelli^{19,e}.

¹*Centro Brasileiro de Pesquisas Físicas (CBPF), Rio de Janeiro, Brazil*

²*Universidade Federal do Rio de Janeiro (UFRJ), Rio de Janeiro, Brazil*

³*Center for High Energy Physics, Tsinghua University, Beijing, China*

⁴*School of Physics State Key Laboratory of Nuclear Physics and Technology, Peking University, Beijing, China*

⁵*University of Chinese Academy of Sciences, Beijing, China*

⁶*Institute Of High Energy Physics (IHEP), Beijing, China*

⁷*Institute of Particle Physics, Central China Normal University, Wuhan, Hubei, China*

⁸*Univ. Grenoble Alpes, Univ. Savoie Mont Blanc, CNRS, IN2P3-LAPP, Annecy, France*

⁹*Université Clermont Auvergne, CNRS/IN2P3, LPC, Clermont-Ferrand, France*

¹⁰*Aix Marseille Univ, CNRS/IN2P3, CPPM, Marseille, France*

¹¹*Universit Paris-Saclay, CNRS/IN2P3, IJCLab, 91405 Orsay, France , Orsay, France*

¹²*LPNHE, Sorbonne Université, Paris Diderot Sorbonne Paris Cité, CNRS/IN2P3, Paris, France*

¹³*I. Physikalisches Institut, RWTH Aachen University, Aachen, Germany*

¹⁴*Fakultät Physik, Technische Universität Dortmund, Dortmund, Germany*

¹⁵*Max-Planck-Institut für Kernphysik (MPIK), Heidelberg, Germany*

¹⁶*Physikalischs Institut, Ruprecht-Karls-Universität Heidelberg, Heidelberg, Germany*

¹⁷*School of Physics, University College Dublin, Dublin, Ireland*

¹⁸*INFN Sezione di Bari, Bari, Italy*

¹⁹*INFN Sezione di Bologna, Bologna, Italy*

²⁰*INFN Sezione di Ferrara, Ferrara, Italy*

²¹*INFN Sezione di Firenze, Firenze, Italy*

²²*INFN Laboratori Nazionali di Frascati, Frascati, Italy*

²³*INFN Sezione di Genova, Genova, Italy*

²⁴*INFN Sezione di Milano-Bicocca, Milano, Italy*

²⁵*INFN Sezione di Milano, Milano, Italy*

²⁶*INFN Sezione di Cagliari, Monserrato, Italy*

²⁷*INFN Sezione di Padova, Padova, Italy*

²⁸*INFN Sezione di Pisa, Pisa, Italy*

²⁹*INFN Sezione di Roma Tor Vergata, Roma, Italy*

³⁰*INFN Sezione di Roma La Sapienza, Roma, Italy*

³¹*Nikhef National Institute for Subatomic Physics, Amsterdam, Netherlands*

³²*Nikhef National Institute for Subatomic Physics and VU University Amsterdam, Amsterdam, Netherlands*

³³*Henryk Niewodniczanski Institute of Nuclear Physics Polish Academy of Sciences, Kraków, Poland*

³⁴*AGH - University of Science and Technology, Faculty of Physics and Applied Computer Science, Kraków, Poland*

³⁵*National Center for Nuclear Research (NCBJ), Warsaw, Poland*

³⁶*Horia Hulubei National Institute of Physics and Nuclear Engineering, Bucharest-Magurele, Romania*

³⁷*Petersburg Nuclear Physics Institute NRC Kurchatov Institute (PNPI NRC KI), Gatchina, Russia*

³⁸*Institute of Theoretical and Experimental Physics NRC Kurchatov Institute (ITEP NRC KI), Moscow, Russia, Moscow, Russia*

³⁹*Institute of Nuclear Physics, Moscow State University (SINP MSU), Moscow, Russia*

⁴⁰*Institute for Nuclear Research of the Russian Academy of Sciences (INR RAS), Moscow, Russia*

⁴¹*Yandex School of Data Analysis, Moscow, Russia*

⁴²*Budker Institute of Nuclear Physics (SB RAS), Novosibirsk, Russia*

⁴³*Institute for High Energy Physics NRC Kurchatov Institute (IHEP NRC KI), Protvino, Russia, Protvino, Russia*

⁴⁴*ICCUB, Universitat de Barcelona, Barcelona, Spain*

⁴⁵*Instituto Galego de Física de Altas Enerxías (IGFAE), Universidade de Santiago de Compostela, Santiago de Compostela, Spain*

⁴⁶*Instituto de Fisica Corpuscular, Centro Mixto Universidad de Valencia - CSIC, Valencia, Spain*

- ⁴⁷European Organization for Nuclear Research (CERN), Geneva, Switzerland
⁴⁸Institute of Physics, Ecole Polytechnique Fédérale de Lausanne (EPFL), Lausanne, Switzerland
⁴⁹Physik-Institut, Universität Zürich, Zürich, Switzerland
⁵⁰NSC Kharkiv Institute of Physics and Technology (NSC KIPT), Kharkiv, Ukraine
⁵¹Institute for Nuclear Research of the National Academy of Sciences (KINR), Kyiv, Ukraine
⁵²University of Birmingham, Birmingham, United Kingdom
⁵³H.H. Wills Physics Laboratory, University of Bristol, Bristol, United Kingdom
⁵⁴Cavendish Laboratory, University of Cambridge, Cambridge, United Kingdom
⁵⁵Department of Physics, University of Warwick, Coventry, United Kingdom
⁵⁶STFC Rutherford Appleton Laboratory, Didcot, United Kingdom
⁵⁷School of Physics and Astronomy, University of Edinburgh, Edinburgh, United Kingdom
⁵⁸School of Physics and Astronomy, University of Glasgow, Glasgow, United Kingdom
⁵⁹Oliver Lodge Laboratory, University of Liverpool, Liverpool, United Kingdom
⁶⁰Imperial College London, London, United Kingdom
⁶¹Department of Physics and Astronomy, University of Manchester, Manchester, United Kingdom
⁶²Department of Physics, University of Oxford, Oxford, United Kingdom
⁶³Massachusetts Institute of Technology, Cambridge, MA, United States
⁶⁴University of Cincinnati, Cincinnati, OH, United States
⁶⁵University of Maryland, College Park, MD, United States
⁶⁶Los Alamos National Laboratory (LANL), Los Alamos, United States
⁶⁷Syracuse University, Syracuse, NY, United States
⁶⁸Laboratory of Mathematical and Subatomic Physics , Constantine, Algeria, associated to ²
⁶⁹School of Physics and Astronomy, Monash University, Melbourne, Australia, associated to ⁵⁵
⁷⁰Pontifícia Universidade Católica do Rio de Janeiro (PUC-Rio), Rio de Janeiro, Brazil, associated to ²
⁷¹Guangdong Provincial Key Laboratory of Nuclear Science, Institute of Quantum Matter, South China Normal University, Guangzhou, China, associated to ³
⁷²School of Physics and Technology, Wuhan University, Wuhan, China, associated to ³
⁷³Departamento de Fisica , Universidad Nacional de Colombia, Bogota, Colombia, associated to ¹²
⁷⁴Institut für Physik, Universität Rostock, Rostock, Germany, associated to ¹⁶
⁷⁵Van Swinderen Institute, University of Groningen, Groningen, Netherlands, associated to ³¹
⁷⁶Universiteit Maastricht, Maastricht, Netherlands, associated to ³¹
⁷⁷National Research Centre Kurchatov Institute, Moscow, Russia, associated to ³⁸
⁷⁸National University of Science and Technology “MISIS”, Moscow, Russia, associated to ³⁸
⁷⁹National Research University Higher School of Economics, Moscow, Russia, associated to ⁴¹
⁸⁰National Research Tomsk Polytechnic University, Tomsk, Russia, associated to ³⁸
⁸¹University of Michigan, Ann Arbor, United States, associated to ⁶⁷

^aUniversidade Federal do Triângulo Mineiro (UFTM), Uberaba-MG, Brazil

^bLaboratoire Leprince-Ringuet, Palaiseau, France

^cP.N. Lebedev Physical Institute, Russian Academy of Science (LPI RAS), Moscow, Russia

^dUniversità di Bari, Bari, Italy

^eUniversità di Bologna, Bologna, Italy

^fUniversità di Cagliari, Cagliari, Italy

^gUniversità di Ferrara, Ferrara, Italy

^hUniversità di Genova, Genova, Italy

ⁱUniversità di Milano Bicocca, Milano, Italy

^jUniversità di Roma Tor Vergata, Roma, Italy

^kAGH - University of Science and Technology, Faculty of Computer Science, Electronics and Telecommunications, Kraków, Poland

^lDS4DS, La Salle, Universitat Ramon Llull, Barcelona, Spain

^mHanoi University of Science, Hanoi, Vietnam

ⁿUniversità di Padova, Padova, Italy

^oUniversità di Pisa, Pisa, Italy

^pUniversità degli Studi di Milano, Milano, Italy

^qUniversità di Urbino, Urbino, Italy

^rUniversità della Basilicata, Potenza, Italy

^sScuola Normale Superiore, Pisa, Italy

^t Università di Modena e Reggio Emilia, Modena, Italy

^u Università di Siena, Siena, Italy

^v MSU - Iligan Institute of Technology (MSU-IIT), Iligan, Philippines

^w Novosibirsk State University, Novosibirsk, Russia

^x INFN Sezione di Trieste, Trieste, Italy

^y School of Physics and Information Technology, Shaanxi Normal University (SNNU), Xi'an, China

^z Universidad Nacional Autonoma de Honduras, Tegucigalpa, Honduras